

# PETs and Polygonal Outer Billiards: Flux, Renormalization, and Compacification

Richard Evan Schwartz \*

April 1, 2026

## Abstract

This article, which loosely follows lectures I gave at Luminy, discusses some ideas about polytope exchange transformations and polygonal outer billiards.

## 1 Introduction

This article is an elaboration on two of the four lectures I gave at C.I.R.M., Luminy, in August 2023. Two of the lectures discussed polygonal outer billiards and piecewise isometric maps. Amongst the piecewise isometric maps I mostly talked about polytope exchange transformations, or PETs. The third lecture discussed ordinary billiards, and the fourth lecture – kind of a wild card topic I threw in at the spur of the moment – discussed a connection between continued fractions and a special case of the Four Color Theorem.

This article will concentrate on the two lectures about polygonal outer billiards and PETs. Aside from considerations of length, let me give some rationale for this choice. First, I recently wrote a survey article that concentrated on ordinary billiards for the Proceedings of the 2022 ICM. See [S1]. Second, the mathematics on the Four Color Theorem is well explicated in my paper [S2]. Third, I am inspired by the popularity of one of the problem

---

\*Supported by N.S.F. Grant DMS-2102802, a Mercator Fellowship, and a Simons Sabbatical Fellowship

sessions I gave at Luminy. This problem session concentrated on a beautiful (and well studied) two dimensional example of a piecewise isometric map. See §2.3. I thought it would be nice to talk more about that kind of mathematics.

Lastly, my involvement with outer billiards is much more extensive than my involvement with the other topics I lectured on. I spent about 7 years of my life really working hard on this topic. I thought it would be nice to give an impressionistic overview of all this work, culminating in a grand but unfulfilled vision of how I see polygonal outer billiards.

I have a wistful feeling as I write this article. While working on outer billiards and PETs, I had the impression that I could spend the rest of my life making fruitful discoveries about it. It was very much like drinking water by putting a fire hose up to your face. I guess that many people working in dynamics, especially experimentally inspired dynamics, would say similar things. However, eventually I abandoned the topic because I wanted to explore other areas of mathematics, to see what else I could do.

This article is structured as follows. In §2 I define what I mean by a piecewise defined map, and then give a bunch of examples. PETs represent the special case when everything is defined in terms of polytopes and the maps are translations. The examples start out easy and familiar and then gradually evolve into more intricate ones. One theme in §2 is the role played by renormalization in understanding the deep structure of the dynamics of these kinds of maps. These maps do not always have a renormalization scheme associated to them, but when they do it is a powerful tool.

In §3 I will discuss polygonal outer billiards, often through examples. One general idea I want to get across is that there is an associated unbounded PET which I call *the pinwheel map*. This map is often easier to understand than outer billiards but, with respect to unbounded orbits, it contains precisely the same information. I will use the structure of the pinwheel map to explain the celebrated result of Vivaldi-Shaidenko [VS], Kolodziej [K], and Gutkin-Simanyi [GS] that all orbits are bounded for so-called quasi-rational polygons. As a corollary, one gets the familiar and very appealing result that all orbits are periodic with respect to a polygon with rational vertices. These results hold for all rational polygons, but my exposition assumes that the polygons have no parallel sides. This makes the discussion easier.

In §4 I will concentrate on my result about unbounded orbits for irrational kites. This is the subject of both my monographs [S3] and [S4]. I hope to give at least a feel for how the results work. The way I will illustrate the

result is through an associated geometric construction called the *arithmetic graph*. This idea is closely related to the *module construction* in [VL]. The final section in §4 discusses some ideas about a general theory of polygonal outer billiards. Many sections in this article illustrate these ideas separately, in simple situations, and then I will try to put them all together.

One thing I would like to say is that almost everything discussed in this article comes from experimentation. I invite the reader to download the software <sup>1</sup> and try it out. Using these programs and seeing the pictures is really the right way to absorb this kind of mathematics. I learned everything from writing and using the programs. If you are having trouble installing and using the software, feel free to send me an email and I will personally help get it to work for you.

I would like to thank C.I.R.M. for their hospitality during my stay there in the summer of 2023. I had a great time. I would especially like to thank Nicolas Bedaride and Jayadev Athreya for inviting me to give these lectures. Some of the ideas about compactification of polygonal outer billiards systems benefitted from discussions with John Smillie. He and I had planned to work on some of this together but somehow never did. I'd like to thank John for those conversations. My work is currently supported by the U.S. National Science Foundation, by a Mercator Fellowship (from Germany) and by a Simons Sabbatical Fellowship. I thank all these institutions for their support.

---

<sup>1</sup>In a few simple cases, as for 3-IETs, my code is not publicly available because it is not a very polished program; I can send it out upon request.

## 2 Piecewise Isometric Maps

### 2.1 General Definitions

It is tempting to give very general definitions of piecewise defined maps, but to avoid pathologies we will almost always work with maps that are piecewise isometries or piecewise translations. In one instance, discussed in §4.3, we will broaden our class of maps and work with piecewise affine maps. See e.g. [Go] for a survey of piecewise isometric maps.

**Piecewise Defined Maps:** A *convex polyhedron* in  $\mathbf{R}^n$  is the convex hull of finitely many points in  $\mathbf{R}^n$ , provided that this convex hull has non-empty interior. A *polyhedral set* in  $\mathbf{R}^n$  is a set which is the finite union of convex polyhedra. Most of our examples will simply be convex polyhedra. Suppose that  $\mathcal{A}$  is some collection of maps which is closed under finite compositions. For instance,  $\mathcal{A}$  could be the set of all real projective maps, or the set of linear fractional maps. (Again, we will almost always take  $\mathcal{A}$  to be the set of isometries or translations of Euclidean space.) A *piecewise- $\mathcal{A}$*  map of  $X$  is given by the following data:

- A union  $X = X_1 \cup \dots \cup X_m$  such that  $X$  and each  $X_i$  is a polyhedral set. Also the various  $X_i$  should have disjoint interiors. We call this decomposition a *partition* of  $X$ .
- A choice  $f_i \in \mathcal{A}$  for all  $i = 1, \dots, m$  such that  $f_i : X_i \rightarrow X$  is well-defined.

We then define  $f : X \rightarrow X$  by the rule  $f(p) = f_i(p)$  when  $p$  lies in the interior of  $X_i$ . The map is undefined on points of  $X$  which do not lie in the interior of some  $X_i$ . We have set things up in such a way that  $f$  is almost everywhere defined in  $X$ . That is,  $f$  is defined except on a set of Lebesgue measure 0.

**Invertibility:** We call  $f$  *invertible* if the maps  $f_i$  are all injective, and  $f_i^{-1} \in \mathcal{A}$ , and the sets  $f_1(X_1), \dots, f_m(X_m)$  form a partition of  $X$ . In this case, the inverse map  $f^{-1}$  is also a piecewise- $\mathcal{A}$  map. All the examples we consider will be invertible. Usually the maps we consider are invertible. In the invertible case,  $f$  is defined in terms of the *first partition*  $X_1, \dots, X_m$  and the *second partition*  $f(X_1), \dots, f(X_m)$ , and the maps between them.

**Periodic Points and Islands:** We denote the  $k$ -fold composition of  $f$

by  $f^k$ . A point  $p \in X$  is *periodic* if  $f^k(p) = p$  for some  $k$ . A subset  $Y \subset X$  is called a *periodic island* if there is some  $k$  such that  $f^k$  is the identity on  $Y$ . Given a periodic point  $p$ , we define the *symbolic sequence* of  $p$  to be the finite sequence  $i_0, \dots, i_{k-1}$  such that  $f^j(p) \in X_{i_j}$ . So, in other words,  $p \in X_{i_0}$  and  $f(p) \in X_{i_1}$ , etc.

**First Return Map:** Given  $Y \subset X$  and a point  $p \in Y$  we can attempt to define the *first return*  $f_{(Y)}(p) \in Y$  to be the first positive iterate  $f^k(p) \in Y$ . Of course, it might happen that this is not defined at all. We say that  $f_{(Y)}$  is *well-defined* if it is a piecewise- $\mathcal{A}$  map.

**Renormalization Sets:** We call  $Y$  a *renormalization set* for  $f$  if the following is true:

- $f_{(Y)}$  is well defined.
- There is some  $k$  such that  $X - Y$  has a partition into finitely many periodic islands and sets of the form  $f^j(Y)$  for  $j \leq k$ .

So, ignoring a set of measure 0, all points  $X$  either belong to periodic islands or else land in  $Y$  after a certain number of iterates. If we ignore the finite number of periodic islands in  $X - Y$ , then the dynamics of  $f$  on  $X$  essentially reduces to the dynamics of  $f_{(Y)}$  on  $Y$ . The kind of situation sometimes gives a lot of information about  $f$ , particularly if we can relate  $f_{(Y)}$  back to  $f$  in some way.

There is one subtlety about this definition that we point out. There may be infinitely many periodic islands in  $X - Y$ , but most of these will live in a set of the form  $f^j(Y)$ . We are ignoring these; they are not part of the partition of  $X - Y$  we mention above.

## 2.2 Interval Exchange Transformations

The simplest maps of the kind we are considering are *interval exchange transformations*. These are often called *IETs* for short. In this case  $n = 1$  and  $X$  is a line segment and  $\mathcal{A}$  is the set of translations of the line. There is an enormous literature on these, and we will only mention a few things. For information about IETs, especially in connection with rational billiards, translation surfaces, and Teichmüller dynamics, see [FM] and [Z] and the references therein.

**General Case:** Let  $S_m$  be the group of permutations on  $\{1, \dots, m\}$ . In general, an interval exchange transformation is defined by three pieces of data: an integer  $m$ , a permutation  $\pi \in S_m$ , and positive numbers  $\lambda_1, \dots, \lambda_m$ . Setting  $\lambda = \lambda_1 + \dots + \lambda_m$ , our initial partition of  $[0, \lambda]$  is given by intervals of lengths  $\lambda_1, \dots, \lambda_m$  ordered from left to right. We then reorder these intervals according to the partition  $\pi$  and obtain a second partition of  $[0, \lambda]$ . The map  $f$  in this instance carries the  $k$ th interval of the first partition to the  $\pi(k)$ th interval of the second partition by a translation. The space of all  $m$ -interval IETs is naturally identified with  $S_m \times \mathcal{C}_m$ , where  $\mathcal{C}_m$  is the strictly positive orthant in  $\mathbf{R}^m$ .

A permutation  $\pi$  is called *irreducible* if  $\pi$  does not preserve any subset  $\{1, \dots, k\}$  of  $\{1, \dots, m\}$  with  $k < m$ . Otherwise we call  $\pi$  *reducible*. Usually we ignore the components of  $S_m \times \mathcal{C}_m$  corresponding to reducible permutations. The corresponding IETs can be understood by breaking them into simpler pieces.

**Rotations:** The simplest example of an interval exchange transformation arises when the unit interval  $[0, 1]$  is divided into two intervals  $[0, \lambda]$  and  $[\lambda, 1]$ . The interval exchange transformation switches the two intervals. In other words,  $f : [0, 1] \rightarrow [0, 1]$  is defined so that  $f(x) = x + (1 - \lambda)$  if  $x \in (0, \lambda)$  and  $f(x) = x - \lambda$  if  $x \in (\lambda, 1)$ . We do not define  $f$  on the endpoints of the intervals. The map  $f$  agrees with the rotation  $f^*(x) = [x - \lambda]$  in  $\mathbf{R}/\mathbf{Z}$  wherever  $f$  is defined. When  $\lambda$  is irrational, every defined orbit of  $f$  is dense. When  $\lambda$  is rational, every defined orbit is periodic.

**Three Interval IETs:** Three interval IETs are still quite special and well understood. Let me describe a nice way to visualise them. A similar idea, in a slightly different context, is considered by [VL].

Let  $\omega = \exp(2\pi i/3)$  be the usual third root of unity. Let  $\nu_k = \omega^{k-1}$ . Thus  $\nu_1, \nu_2, \nu_3$  are the three third roots of unity. Given a point  $p \in [0, \lambda]$  with a well defined orbit we first assign the integer *symbolic sequence*  $i_0, i_1, i_2, \dots$  such that  $f^k(p)$  lie in the  $i_k$ th interval. We define

$$z_k = \nu_{i_0} + \dots + \nu_{i_k}, \quad k = 0, 1, 2, \dots \quad (1)$$

Thus we define a path  $z_0 \rightarrow z_1 \rightarrow z_2, \dots$  in the plane which chooses its direction to turn based on the itinerary of the orbit. Call this path  $\Pi(p)$ .

The path  $\Pi(p)$  is not quite embedded. However, here is an interesting phenomenon. We define the *drift vector*

$$d = \sum_{i=1}^3 \lambda_i \nu_i. \quad (2)$$

We then define the modified path  $\Pi_\epsilon(p)$  so that its vertices are  $z'_0, z'_1, z'_2, \dots$  with

$$z'_k = z_k + d\epsilon. \quad (3)$$

We are giving the path  $\Pi(p)$  a little push in the direction  $d$  and calling the new path  $\Pi_\epsilon(p)$ . This is something I noticed computationally, and just for fun. I would not be surprised if the result is known, though I don't know a reference. Let me show some pictures, when  $\epsilon = .3$ . In each case, the black part of the path corresponds to one period, and then the lighter grey part is the periodic continuation.

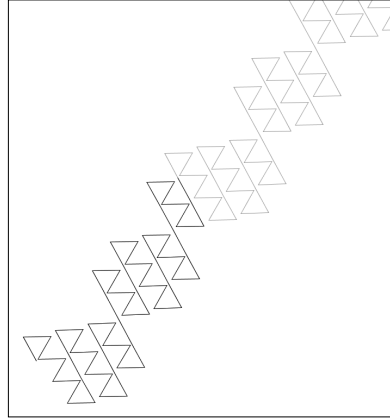


**Figure 2.1:**  $\pi = (13)$  and  $\vec{\lambda} = (24/64, 23/64, 17/64)$ .

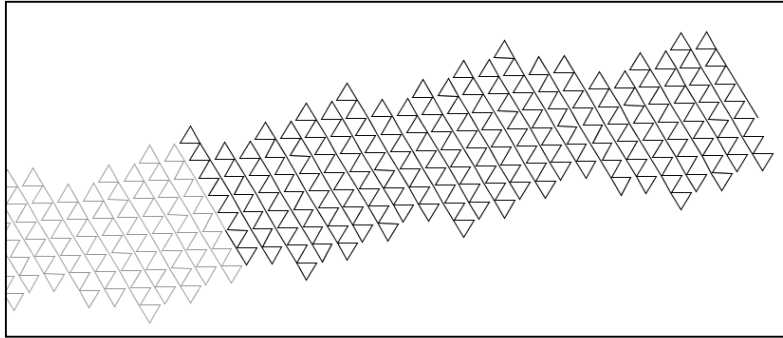


**Figure 2.2:**  $\pi = (13)$  and  $\vec{\lambda} = (157/512, 175/512, 180/512)$ .

The reader might enjoy writing a program that codes up this construction, as I have done. My own software for this – a fairly crude program – is available upon request.

**Generic Minimality:** The literature on IETs is enormous, and there are many, many structural results. Here is one that relates well to the rest of the material in this article.

**Theorem 2.1** *If  $\pi$  is an irreducible permutation then almost every point in  $\{\pi\} \times \mathcal{C}_n$  gives rise to an IET in which every defined orbit is dense.*

This is a corollary of the two lemmas in more precise lemmas in M. Keane’s paper [Ke, §3]. When  $\pi$  is reducible, one could break the corresponding IETs into suitable pieces and make a similar statement about each irreducible piece. So, at least generically, there are no periodic islands.

**Rauzy Induction:** Now we mention a second property that relates well to the material here. The second property is a general renormalization scheme called *Rauzy renormalization* or *Rauzy induction*. See [R] for the original source; there are also many other articles which use Rauzy induction. Let  $f$  be an  $n$ -interval IET. There are three cases to consider:

- If the last interval of the first partition is shorter than the last interval of the second partition. We define  $\rho(f)$  to be the first return map of  $f$  to the first  $n - 1$  intervals of the first partition. This union is a renormalization set.
- If the last interval of the second partition is shorter than the last interval of the first partition. We define  $\rho(f)$  to be the first return map of  $f$  to the union of the first  $n - 1$  intervals of the second partition. This union is a renormalization set.
- Otherwise we do not define  $\rho(f)$ .

Rauzy proves the following result.

**Theorem 2.2**  *$\rho(f)$  is another  $n$ -interval IET. On each component of  $S^n \times \mathcal{C}_n$ , the map  $\rho(f)$  is either entirely undefined or else almost everywhere defined and piecewise affine.*

### 2.3 The Isosceles Triangle Example

A slightly more general situation, one we consider in this section is where  $\mathcal{A}$  is the set of all isometries of  $\mathbf{R}^2$ . See [Go] for another discussion of this example. Comparing the discussion here to the general case discussed in §2.1, we switch notation somewhat so that  $X = T_0$  and  $(X_1, X_2) = (T_1, U_1)$ . Let  $T_0$  be an isosceles triangle with side lengths  $1, \phi, \phi$ , where  $\phi = (1 + \sqrt{5})/2$  is the golden ratio. The left side of Figure 2.3 shows how one can use a regular pentagon as scaffolding to draw  $T_0$  and also a partition of  $T_0$  into two smaller isosceles triangles  $T_1$  and  $U_1$ .

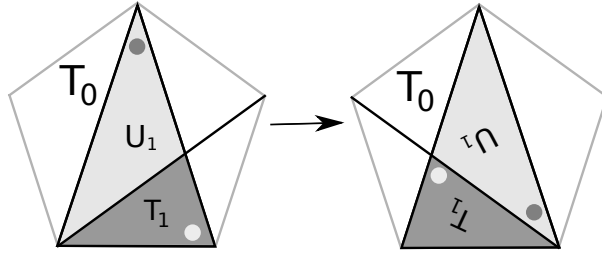


**Figure 2.3:** The partition of  $T_0$  into  $T_1$  and  $U_1$ .

The right side of Figure 2.3 shows a second partition of  $T_0$  into two smaller isosceles triangles. The rotated labeling is deliberate. We map  $T_1$  and  $U_1$  to their counterparts by rotations. The rotated labels and dots indicate this. This piecewise rotation is defined everywhere on  $T_0$  except for the interface  $T_1 \cap U_1$ . The resulting map  $f$  is an example of an invertible piecewise isometry.

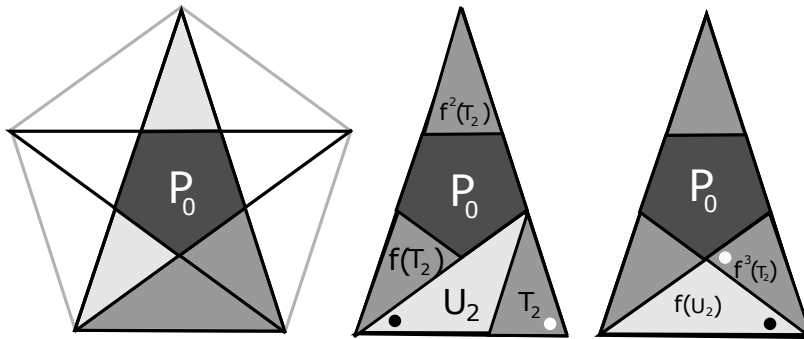


**Figure 2.4:** The periodic island  $P_0$  and the first return map  $f|_{(T_1)}$ .

The left side of Figure 2.4 shows a regular pentagon  $P_0$  which is a periodic island. The iterate  $f^5$  acts as the identity on  $P_0$ .

Let's look at the middle and left part of Figure 2.4. The triangle  $T_1$  breaks into two smaller pieces  $T_2$  and  $U_2$ . The first return map  $f|_{(T_1)}$  is well defined, and there is some additional structure. There is a similarity  $\phi : T_1 \rightarrow T_0$  such that

$$f_{(T_1)} = \phi^{-1} \circ f \circ \phi. \quad (4)$$

Furthermore, we have the partition.

$$U_1 - P_0 = f(T_2) \cup f^2(T_2). \quad (5)$$

All this says that  $T_1$  is a renormalization set for  $f$ . Moreover, the action of the first return map  $f_{(T_1)}$  on  $T_1$  is a smaller copy of the action of  $f$  on  $T_0$ . The map  $\phi$  is responsible for the copy of the periodic islands in  $T_0$  to  $T_1$ . In particular,  $\phi(P_0)$  is a periodic island in  $U_2$ . This structure lets us show the existence of a dense set of periodic islands.

**Theorem 2.3** *The map  $f$  has a dense set of periodic islands.*

**Proof:** First, if we see a certain pattern of periodic islands in  $T_0$  then we can shrink and copy that pattern and put it inside  $T_1$ . Second, we can use  $f$  and  $f^2$  to transport any pattern of periodic islands in  $T_2$  to a pattern in  $f(T_2)$  and  $f^2(T_2)$ . Figure 2.5 shows this in action.

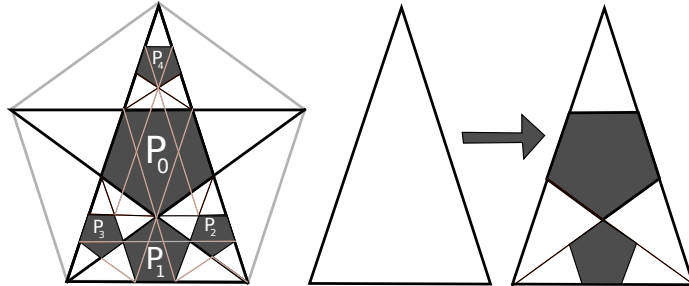


**Figure 2.5:** Recursively constructing periodic islands

The left side of Figure 2.5 shows some more periodic islands whose existence is implied by the two rules above.  $P_1$  is a smaller copy of  $P_0$ , and then  $P_2$  is a smaller copy of  $P_1$ . Finally,  $P_3$  and  $P_4$  are images of  $P_2$  under  $f$  and  $f^2$  respectively. We have added some additional line segments to illustrate how these islands may be constructed just using a ruler. Continuing this analysis in an inductive way, we produce a dense set of pentagonal periodic islands. ♠

The middle and right pictures in Figure 2.5 show a subdivision rule which breaks an isosceles triangle into two pentagons and 5 smaller isosceles triangles of the same shape. As a challenge to the reader, try proving that the above process produces all periodic islands. One idea for a proof is that a spurious periodic island at some scale – meaning one not produced by the process – would come from a spurious periodic island at a larger scale, and so there would have to be a very large spurious periodic island.

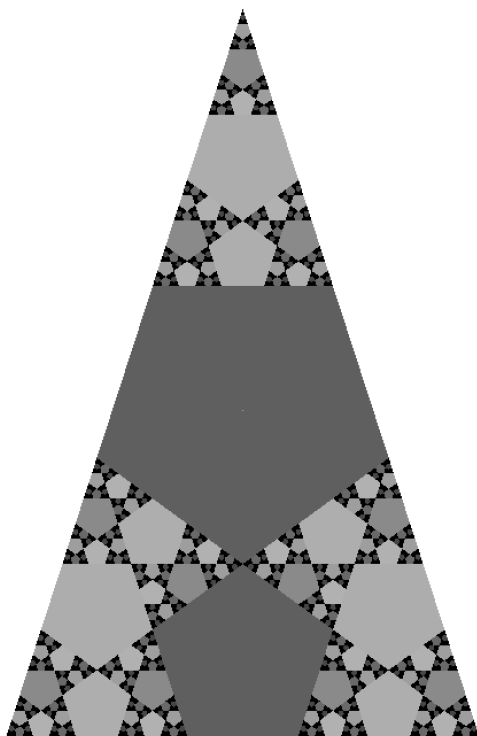


**Figure 2.6:** The biggest periodic islands

Figure 2.6 plots all the periodic islands having period less than 1275. The islands are shaded randomly, based on a random number that is associated to each possible period. The computer-adept reader might be interested in plotting this picture with some other coloring scheme – e.g. one in which the coloring corresponds in some way to the lengths of the periods. Generally, the periods are longer for the smaller islands. One can also deduce the period lengths exactly from the Mathematica code I include below.

**Visualization:** There is a neat way to visualize the dynamics of this map. I don't know if this method has been studied by other authors but in some ways it is related to the module construction in [VL]. We associate to each orbit the symbolic sequence using the numbers  $\{1, 4\}$ .

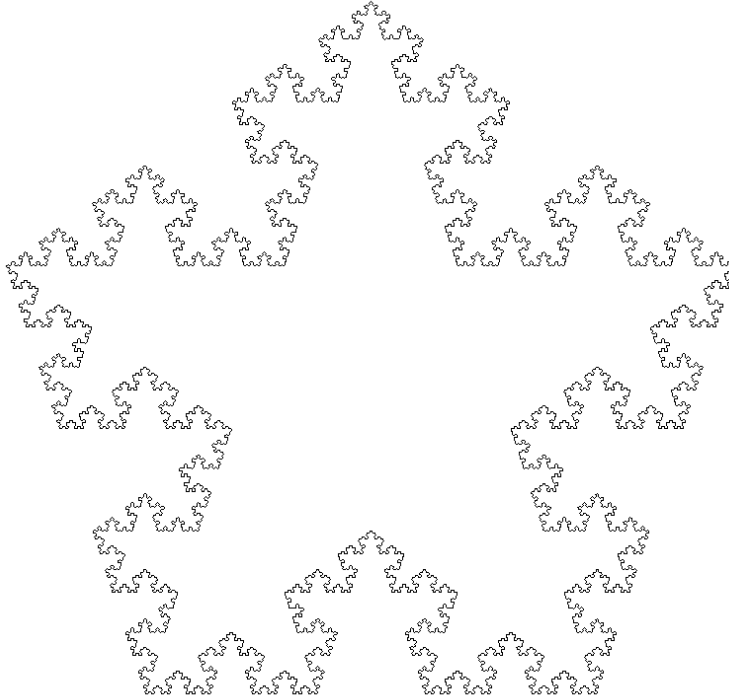


**Figure 2.7:** The curve associated to a long periodic orbit.

We assign a 2 when the orbit lies in  $T_1$  and a 3 when the orbit lies in  $U_1$ . Call this sequence  $m_0, m_1, m_2, \dots$ . We set  $n_k = (m_0 + \dots + m_k) \bmod 5$ . We then let  $\zeta_k = \omega^{n_k}$  where  $\omega = \exp(2\pi i/5)$ . The number  $\zeta_k$  is the Galois conjugate of the unit complex number which computes the local rotation of the map  $f^k$  applied to the initial point. Finally, we associate to the orbit the polygon whose successive vertices are  $\zeta_0, \zeta_0 + \zeta_1, \zeta_0 + \zeta_1 + \zeta_2$ , etc. Figure 2.7 shows what a long periodic orbit looks like.

I don't have a good conceptual understanding of why this curve looks like it does, but I know how to generate these curves in Mathematica and probably also how to prove that they are embedded and fractal-like. The following Mathematica code generates the same curve as above. This follows from the renormalization structure.

```

ClearAll["Global`*"];
ITER=4;
f[1]:={-1,1,1,1,-1};
f[-1]:={-1,1,-1};
g1[A_]:=Flatten[Table[f[A[[j]]],{j,1,Length[A]}]]
h0[A_]:=Table[Sum[A[[j]],{j,1,k}],{k,1,Length[A]}];
h1[a_]:=Exp[2 Pi a I/5];
h2[A_]:=Table[h1[A[[j]]],{j,1,Length[A]}];
h4[A_]:=list=h2[h0[A]];
list2=Table[Sum[list[[j]],{j,1,k}],{k,1,Length[A]}];
list3=Table[{Re[list2[[j]]],Im[list2[[j]]}],{j,1,Length[list2]}];
uu=h4[Nest[g1,{-1,-1,-1,-1,-1},ITER]];
Graphics[Polygon[uu]]

```

I have simply pasted in working Mathematica code, because my attempts to describe it indirectly are likely to introduce errors. If you want to see more or less detailed pictures, and both kinds of pictures, you can change the value of ITER, and/or change the seed from  $\{-1, -1, -1, -1, -1\}$  to  $\{1, 1, 1, 1, 1\}$ .

The symbolic dynamics of the periodic orbits comes from iterating the substitution rules

$$1 \rightarrow (-1, 1, 1, 1, -1), \quad -1 \rightarrow (-1, 1, -1).$$

The initial seeds are  $\pm(1, 1, 1, 1, 1)$ . The periods of the periodic islands are the lengths of the strings you get by iterating this rule finitely many times.

## 2.4 Sublattice PETs

When we take the collection  $\mathcal{A}$  of maps to be the set of translations of  $\mathbf{R}^n$  and insist that  $X$  and its partitions are all convex polytopes, we get a *polytope exchange transformation*, or *PETs* for short. Here I describe a general construction of PETs I made in [S6] and [S7]. This construction uses lattices and sublattices in  $\mathbf{R}^n$ .

A *sublattice* in  $\mathbf{R}^n$  is the  $\mathbf{Z}$ -span of a list of  $k \leq n$  linearly independent vectors. Here  $k$  is the *rank* of the sublattice. When  $k = n$ , a sublattice is known as a *lattice*. A *fundamental domain* for a sublattice  $L$  is a subset  $X \subset \mathbf{R}^n$  such that union of translates of  $X$  by  $L$  gives a partition of  $\mathbf{R}^n$ . For instance, the unit cube  $[0, 1]^n$  is a fundamental domain for  $\mathbf{Z}^n$ . One typical example we consider is that of a parallelotope fundamental domain

for a lattice. Another example we consider is an infinite strip fundamental domain for a rank one sublattice in  $\mathbf{R}^2$ . Every sublattice has infinitely many fundamental domains. Likewise, every paralleloiped fundamental domain for a sublattice is the fundamental domain for infinitely many such.

Given a sublattice  $L$  and a fundamental domain  $X$  we have a mapping

$$\pi_{X,L} : \mathbf{R}^n \rightarrow X.$$

Given  $p \in \mathbf{R}^n$ , the point  $\pi_{X,L}(p)$  lies in  $X$  and differs from  $p$  by a member of  $L$ . For almost all  $p \in \mathbf{R}^n$  this map is uniquely defined. For all other points we leave the map undefined.

Suppose now that  $\Gamma$  is a finite bipartite graph, with black and white vertices. We say that a *decoration* of  $G$  is an assignment of a sublattice to each white vertex and a subset of  $\mathbf{R}^n$  to each black vertex with the following property: For each edge, the set associated to the black vertex is a fundamental domain for the sublattice associated to the white vertex.

We now consider paths in  $\Gamma$  that start at black vertices. Suppose that  $\gamma$  is a length 2 path in  $\Gamma$ , whose consecutive vertices are  $b_0, w_1, b_2$ . Let  $X_0, L_1, X_2$  be the corresponding decorations. We have a canonical piecewise isometry  $X_0 \rightarrow X_2$  defined as the composition

$$\phi_\gamma = \phi_{b_2, w_1, b_0} = \pi_{X_2, L_1} \circ \iota, \tag{6}$$

where  $\iota$  is the inclusion map from  $X_0$  to  $\mathbf{R}^n$ . More generally, if  $\gamma$  is a length  $2n$  path with vertices  $b_0, w_1, \dots, b_{2n}$  then we have the composition

$$\phi_\gamma = \phi_{b_{2n}, w_{2n-1}, b_{2n-1}} \circ \dots \circ \phi_{b_2, w_1, b_0}. \tag{7}$$

When  $\gamma$  is a loop, meaning that  $b_{2n} = b_0$ , the map  $\phi_\gamma$  is a PET defined on  $X_0$ . The inverse of the map is given by  $\phi_{\gamma^{-1}}$ , where  $\gamma^{-1}$  is the same loop as  $\gamma$  but traced in the reverse order.

One case we specially consider is as follows:

- $\Gamma$  is a 4-cycle.
- $\gamma$  is a loop that traverses all 4 vertices.
- The white vertex decorations are lattices.

In this case, we call  $\phi_\gamma$  a *double lattice PET*. We have two lattices and two fundamental domains for them. We consider such examples in the next section. We also discuss double lattice PETs in §4.

## 2.5 The Octagonal PETs

Now I will specialize the discussion above to a 1-parameter family of 2-dimensional double lattice PETs. These are the main objects in [S7].

Given  $s \in \mathbf{R}$ , the two fundamental domains are

$$X_0 = \langle (2s, 2s), (2, 0) \rangle, \quad X_2 = \langle (-2s, 2s), (0, 2) \rangle. \quad (8)$$

Here  $\langle v_1, v_2 \rangle$  denotes the parallelogram with vertices  $\pm v_1/2 \pm v_2/2$ . Figures 2.8 and 2.8 below give an idea of what  $X_0$  looks like. We get  $X_2$  by rotating  $X_0$  by 90 degrees about its center point.

The two lattices are

$$L_1 = \{(2s, 2s), (0, 2)\} \quad L_3 = \{(-2s, 2s), (-2, 0)\} \quad (9)$$

Here  $\{v_1, v_2\}$  denotes the  $\mathbf{Z}$ -span of  $v_1$  and  $v_2$ . These two lattices are also 90-degree rotations of each other. Each parallelogram is a fundamental domain for each lattice, and so the map  $f_s$ , defined by the loop  $b_0, w_1, b_2, w_3$  is a double lattice PET.

A *semi-regular octagon* is a convex polygon one gets by cutting off the four corners of a square in a completely symmetric way. The square itself counts as a semi-regular octagon.

In [7] we prove the following result.

**Theorem 2.4**  *$f_s$  has a dense set of periodic islands for any  $s \in \mathbf{R}$ . These periodic islands are either right-angled isosceles triangles or semi-regular octagons. When  $s$  is irrational, there are no triangles. For a generic choice of  $s$ , one sees a dense set of shapes of semi-regular octagons amongst the set of periodic islands.*

Here is the picture for  $s = \sqrt{2}/2$ . All the periodic islands are regular octagons. This picture is reminiscent of Figure 2.6, and there is a similar renormalization scheme, discussed below, that is responsible for this structure of periodic islands.

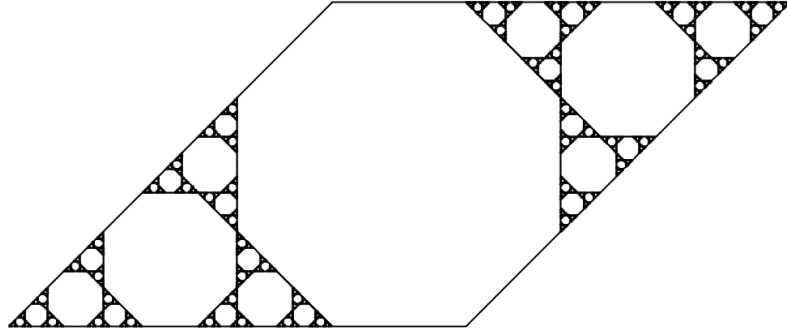


**Figure 2.8:** The periodic islands for  $s = \sqrt{2}/2$ .

Here is a picture for  $s = \sqrt{3}/2 - 1/2$ . This time all the periodic islands are squares. I have shaded them in to indicate the two different ways the squares are oriented in the plane. The interface between the squares is a union of two continuous embedded arcs.

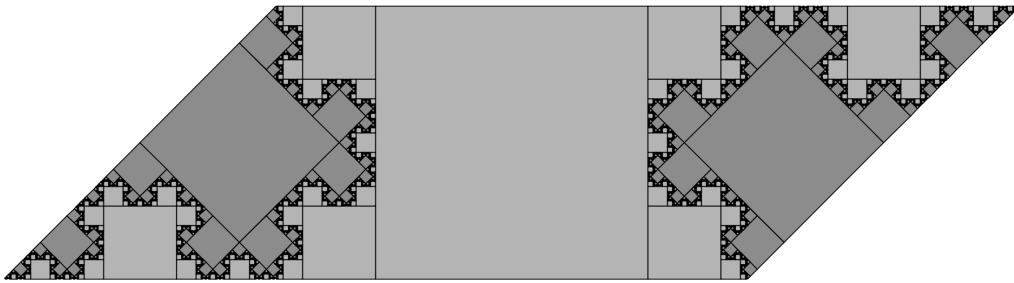


**Figure 2.9:** The periodic islands for  $s = \sqrt{3}/2 - 1/2$ .

If we think of this picture as living on a torus rather than on a parallelogram, then the two arcs piece together to make a continuous embedded loop. The restriction of  $f_s$  to this loop is conjugate to an irrational rotation (wherever it is defined). A renormalization scheme is also responsible for all this structure.

Now we explain how the renormalization scheme works for this 1-parameter family. We define  $R : (0, 1) \rightarrow [0, 1)$  as follows:

- $R(s) = 1 - s$  if  $s > 1/2$ .
- $R(s) = 1/(2s) - \text{floor}(1/(2s))$  if  $s < 1/2$ .

Recall that  $f_s : X_{0,s} \rightarrow X_{0,s}$  is our PET. We let  $Y_{0,s} = X_{0,s} - X_{2,s}$ . In Figures 2.8 and 2.9, the set  $Y_{0,s}$  is the complement of the central tile in the picture. This set has two components in all cases. The intersection  $X_{0,s} \cap X_{2,s}$  is always a semi-regular octagon and a periodic island. So, we omit this periodic island to get  $Y_{0,s}$ .

Let  $t = R(s)$ . Here is the main result of [S7].

**Theorem 2.5 (Renormalization)** *There is a renormalization set  $Z_s \subset Y_s$  together with a piecewise similarity  $\phi_s : Z_s \rightarrow Y_t$  which conjugates the map  $f_s|_{Z_s}$  to the map  $f_t|_{Y_t}$ . The map  $\phi_s$  is a similarity on each of the two symmetrically placed components of  $Z_s$ .*

We illustrate this result with the same pictures that we use in [S7]. We are not showing the dynamics, but rather the collection of periodic islands. Comparing the pictures in Figures 2.10a and 2.10b, and then again in Figures 2.11a and 2.11b, one can get a sense of what the Renormalization Theorem says. The details are worked out in great detail in [S7].

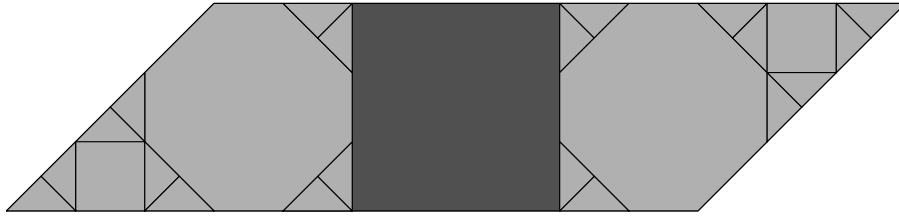


**Figure 2.10a:**  $Y_t$  shaded for  $t = 3/10 = R(5/13)$ .



**Figure 2.10b:**  $Z_s$  shaded  $s = 5/13$ .

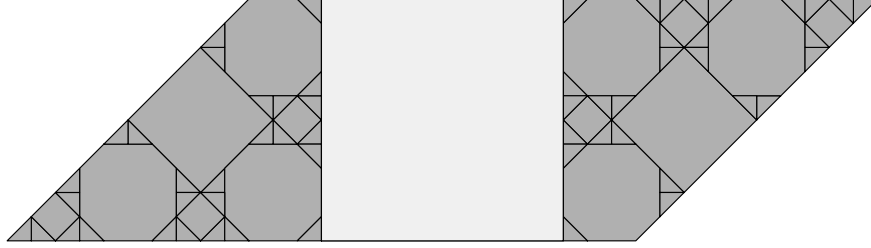


**Figure 2.11a:**  $Y_t$  shaded for  $t = R(8/13) = 5/13$ .

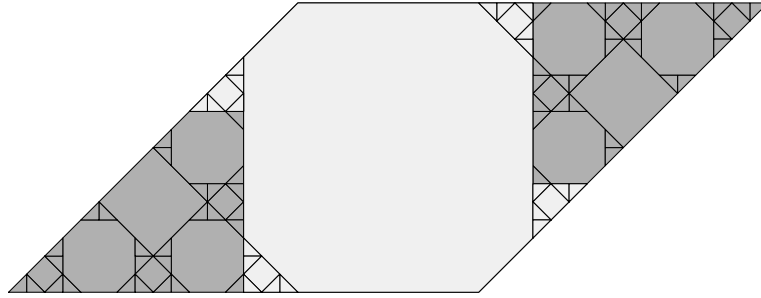


**Figure 2.11b:**  $Z_s$  shaded for  $s = 8/13$ .

The self-similar nature of the periodic islands for  $s_0 = \sqrt{2}/2$  comes from the fact that  $R^2(s_0) = s_0$ . The self-similar nature of the periodic islands for  $s_1 = \sqrt{3}/2 - 1/2$  comes from the fact that  $R(s_1) = s_1$ . In general, any quadratic irrational parameter is pre-periodic under  $R$  and exhibits the same kind of self-similar behavior, albeit more complicated. The typical orbit of  $s$  under  $R$  is dense in  $[0, 1]$ . This accounts for our statement that for generic choice of  $s$ , one sees a dense set of shapes of semi-regular octagon amongst the periodic islands.

The most significant property of  $R$  is that the orbit of any rational number under  $R$  is finite and ends at  $1/2$ . The map  $R$  decreases the sum of the numerator and the denominator. For instance, the  $R$ -orbit of  $5/13$  is

$$5/13 \rightarrow 3/10 \rightarrow 2/3 \rightarrow 1/3 \rightarrow 1/2.$$

The reduction property combines with the Renormalization Theorem to help analyze the action of  $f_s$ . For instance, we can predict exactly the shapes of the periodic islands of  $f_s$  for  $s$  and rational number. See [S7] for details.

## 2.6 PETs Constructed from Strips

Suppose now we have a bipartite graph which is a  $2n$ -cycle. Suppose that to the black vertices we have associated infinite strips  $\Sigma_0, \Sigma_2, \dots, \Sigma_{2n-2} \subset \mathbf{R}^2$ . We insist that cyclically consecutive strips are not parallel.

For each odd index  $k$  there are two rank-1 sublattices having both strips  $\Sigma_{k-1}$  and  $\Sigma_{k+1}$  as fundamental domains. Both choices have the form  $\mathbf{Z}v_k$  where  $v_k$  is a vector which is the difference between a pair of opposite vertices of the parallelogram  $\Pi_k = \Sigma_{k-1} \cap \Sigma_{k+1}$ .

We suppose that the  $k$ th white vertex is decorated by one of these sublattices. So, up to  $2^k$  choices, our strips define for us a sublattice PET.

**Quasi-Rationality:** There is an equivalence amongst these sublattice PETs. If  $A$  is any affine transformation, then the strips  $A(\Sigma_0), \dots, A(\Sigma_{2n-2})$  define an affinely conjugate PET provided that we make the correct choices for the sublattices. We say that the PET is *quasi-rational* if  $A$  may be chosen so that all the parallelograms considered above have integer area. This notion is closely related to the notion of quasi-rationality in polygonal outer billiards. We will discuss this in the next chapter.

**Parallelogram Rotations:** There is an alternate way to view these kinds of PETs. Each planar parallelogram is preserved by an order 4 group of affine symmetries. For the square this is just the group of rotations of the square. In general, we say that the order 4 affine symmetry that rotates counter-clockwise by “one click” is the *fundamental rotation* of the parallelogram, even though it is only a rotation in the affine sense.

Say that a *parallelogram tiling* of an infinite strip  $\Sigma$  is a partition of  $\Sigma$  into parallelograms which are all translates of each other. Say that a *parallelogram map* of  $\Sigma$  is the piecewise affine map obtained by applying the fundamental rotation to each parallelogram separately. It is a fun exercise to show that PETs we have constructed here are compositions of  $n$  parallelogram maps of the strip  $\Sigma_0$ .

In the quasi-rational case, the parallelogram widths are all commensurable, and we can scale so that they are integers. In this case, all the parallelogram tilings are simultaneously invariant under a single translation. This fact is the key to understanding quasi-rational outer billiards.

## 3 Polygonal Outer Billiards

### 3.1 Basic Definitions

Outer billiards goes back at least to B. Neumann's short article [N]. J. Moser considered outer billiards as a toy model for planetary motion [M1], [M2]. I will concentrate on the case of polygons.

Polygonal outer billiards is a piecewise isometric map of  $\mathbf{R}^2$  that is based on a convex polygon  $P \subset \mathbf{R}^2$ . Given a point  $p_0 \in \mathbf{R}^2 - P$  one defines  $p_1 = f(p_0)$  to be the point such that the line segment  $\overline{p_0 p_1}$  is tangent to  $P$  uniquely at its midpoint, and a person walking from  $p_0$  to  $p_1$  would see  $P$  on the right. Figure 3.1 shows the construction.

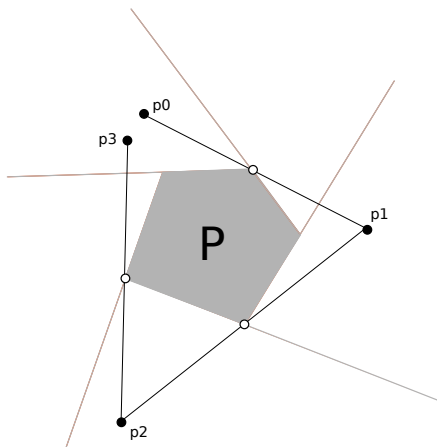


Figure 3.1: Definition of outer billiards

The points  $p_1, p_2, p_3, \dots$  are the forward iterates of  $p_0$  under the outer billiards map. The map is defined in the complement of the grey rays which emanate from the edges of  $P$  like a pinwheel. The inverse map is defined by a similar construction, with the words *left* and *right* swapped. For any  $n$ , the first  $n$  iterates of  $f$ , both forwards and backwards, are defined in the complement of a finite union of lines. In particular, the full orbit of the map is defined in the complement of a countable union of lines.

It is sometimes nicer to consider the square map  $f^2 = f \circ f$  instead. This map is a piecewise translation. We note that, while the iterates of  $f$  tend to circulate clockwise around  $P$ , the iterates of  $f^2$  tend to circulate counterclockwise. This effect is more dramatic if you consider the action on points far away from  $P$ .

### 3.2 Some Examples

**Triangles and Parallelograms:** Outer billiards is an affinely natural system. If  $A$  is an affine transformation, then  $A$  conjugates the outer billiards map with respect to  $P$  to the one with respect to  $A(P)$ . Thus, for instance, one can understand outer billiards with respect to any triangle by understanding the equilateral triangle case. Likewise, one can understand outer billiards with respect to any parallelogram by understanding the square case. For the case of equilateral triangles, the initial triangle extends to the usual tiling of  $\mathbf{R}^2$  by equilateral triangles. Each of these tiles is a periodic island. The square case has a similar description in terms of the square tiling.

**The Regular Pentagon:** Here is what outer billiards looks like on the regular pentagon.

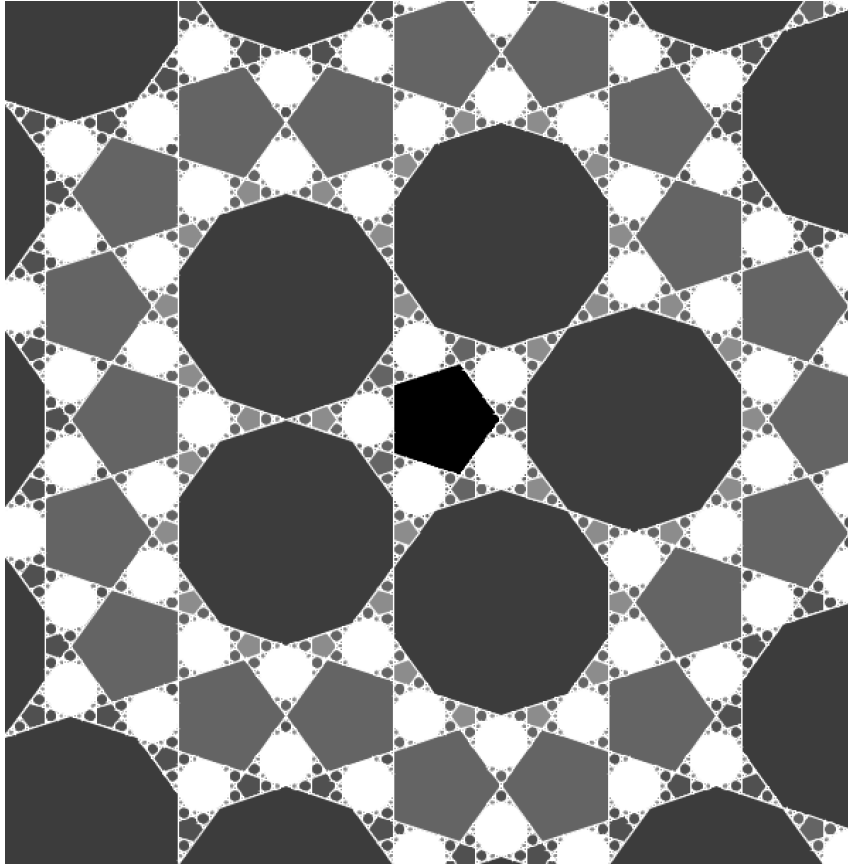


Figure 3.2: Outer billiards on the regular pentagon

The structure in this case is first analyzed in [T2]. Here is a consequence of the work in [T2].

**Theorem 3.1** *With respect to outer billiards on the regular pentagon, there is a dense set of periodic islands, either regular pentagons or regular decagons. Moreover, there is an infinite union of “pentagon necklaces” made from pentagons isometric to the central one. These necklaces alternate with an infinite union of “decagon necklaces”. Finally, there exist some aperiodic orbits.*

Figure 3.2 just shows the first of each necklace, and about half of the second decagon necklace.

Between these necklaces there is a self-similar pattern that is reminiscent to the isosceles triangle example considered in §2.3. S. Tabachnikov establishes this self-similar property using a similar kind of renormalization scheme. The picture between consecutive decagon necklaces is essentially independent of the position. To say this somewhat more precisely, we can consider the intersection of the picture with a horizontal strip. Once we go sufficiently far out to the right, the picture becomes periodic. Figure 3.3 illustrates what we mean.

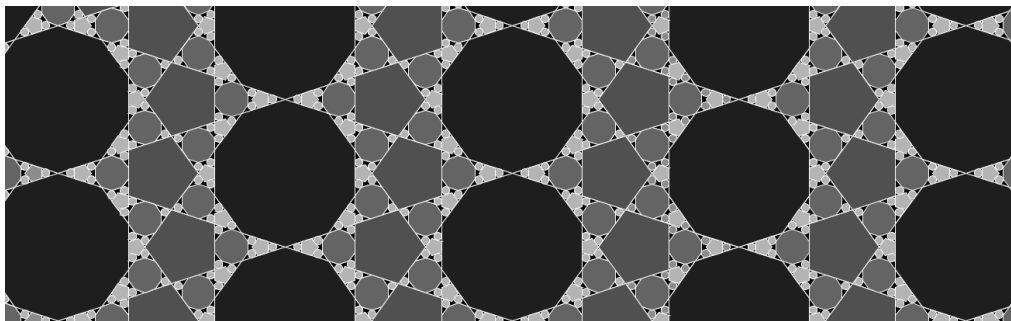


**Figure 3.3:** Outer billiards (again) on the regular pentagon

**The Regular Octagon:** Figure 3.4 shows some of the periodic islands for outer billiards on the regular octagon. Once again we have an infinite sequence of octagon necklaces with a fractal pattern in between them. We are showing the innermost later. Notice that the pattern inside the highlighted parallelogram exactly matches the one in Figure 2.8. Considered as a semi-regular octagon, the regular octagon has parameter  $s = \sqrt{2}/2$ .

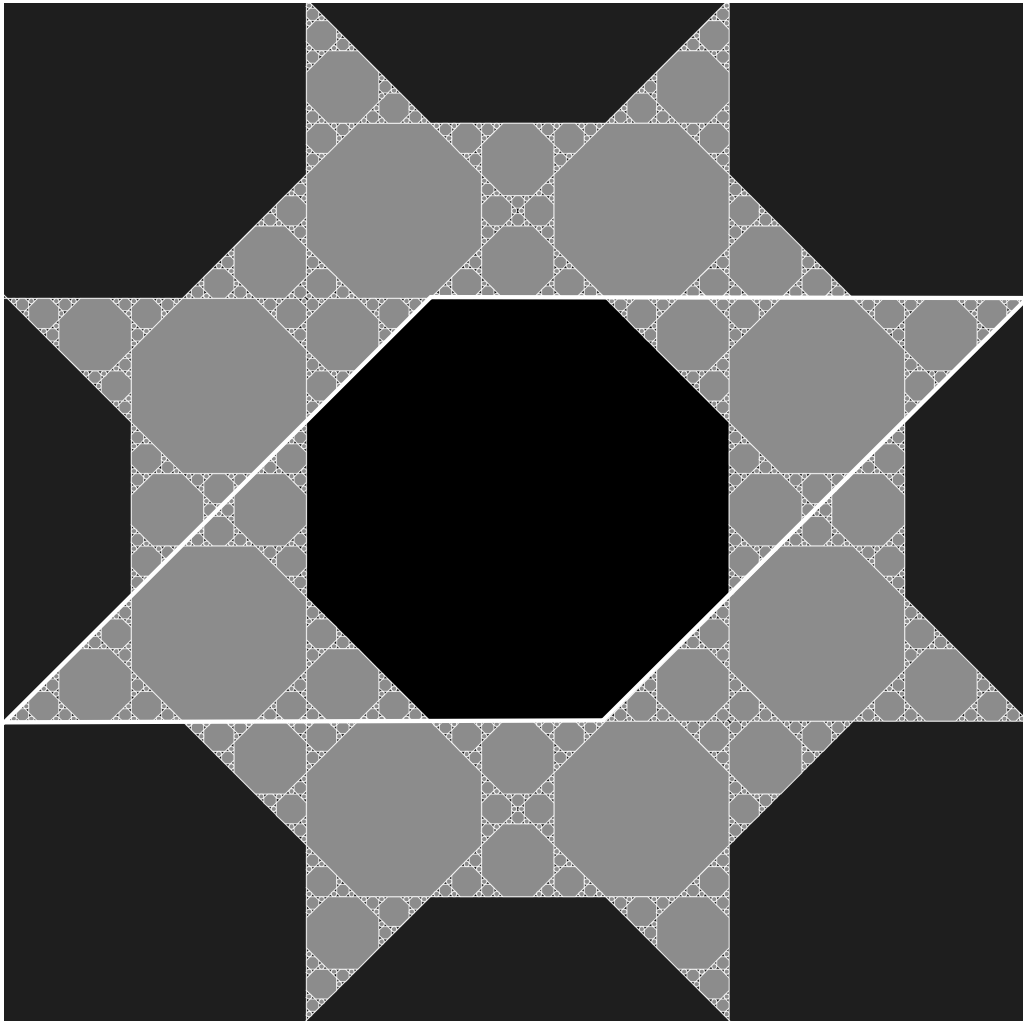


**Figure 3.4:** Outer billiards on the regular octagon

**Semi-Regular Octagons:** Figure 3.5 shows outer billiards with respect to the semi-regular octagon with parameter  $s = 3/2 - \sqrt{3}/2$ . Again, we are just showing the inner layer. The fractal pattern that lives between the octagon necklaces matches the one for the octagonal pet with the same parameter. The given parameter  $s$  is such that  $R(s)$  is the parameter for the Octagonal PET shown in Figure 2.9. You can see the close resemblance. Were we to plot the picture for the pet  $f_s$  with  $s = 3/2 - \sqrt{3}/2$  we would get exactly the picture inside the white parallelogram.

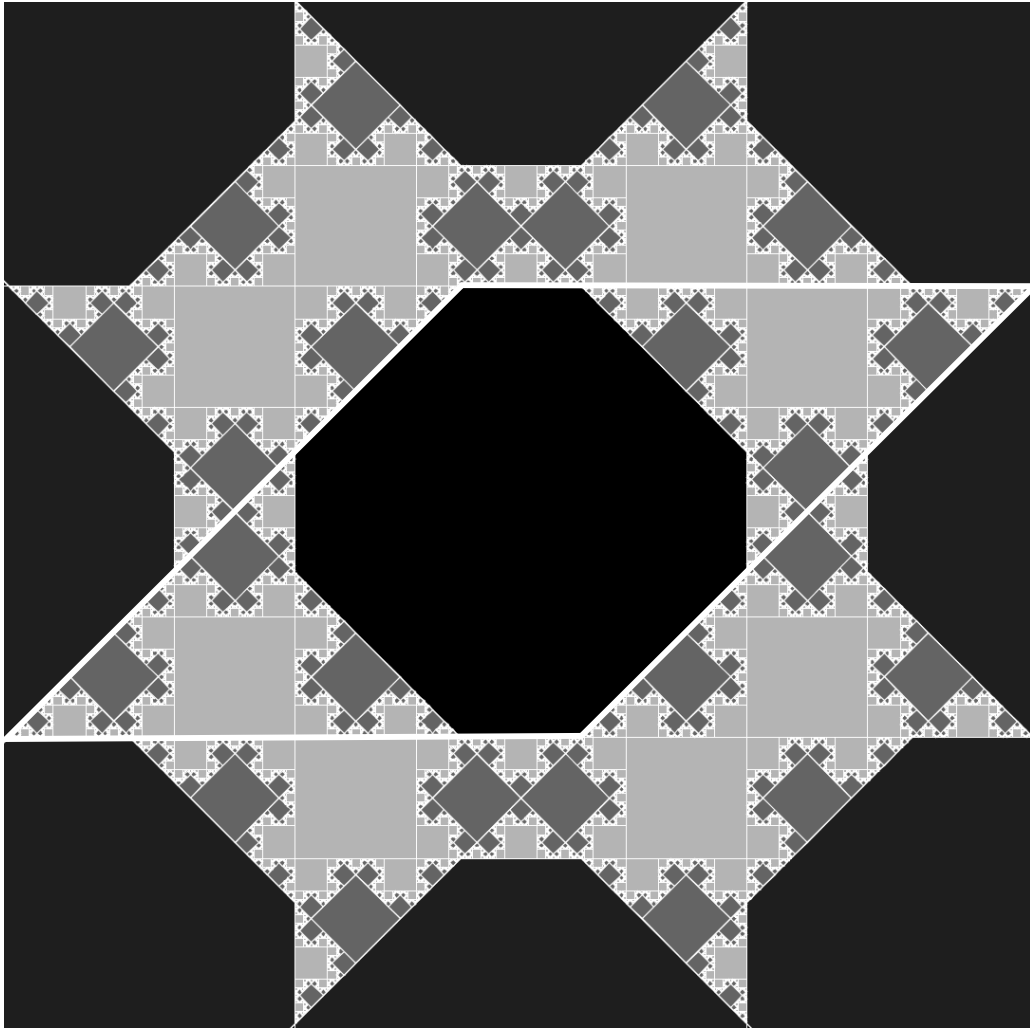


**Figure 3.5:** Outer billiards on the regular octagon

Let  $O(s)$  be the semi-regular octagon with parameter  $s \in (1/2, 1)$ . We proved in [S7] that outer billiards with respect to  $O(s)$  produces a pattern of periodic islands that is locally the same as the pattern produced by the octagonal PET with parameter  $s$ . More precisely,

**Theorem 3.2** *The complement  $\mathbf{R}^2 - O(s)$  is tiled by congruent parallelograms, each isometric to  $X_{0,s}$ , such that the shapes and the arrangement of periodic islands in each of these parallelograms is the same as that in  $X_{0,s}$ .*

The dynamics of outer billiards is not quite the same as the dynamics in the corresponding octagonal PET. The two systems are “commensurable” in

a sense made precise in [S7]. In any case, the octagonal PETs control the structure of the periodic islands for outer billiards in semi-regular octagons.

There is an important point to note. The octagon  $O(s)$  is only defined when  $s \in (1/2, 1)$  and the octagonal PETs are defined when  $s \in (0, 1)$ . Our renormalization scheme for octagonal PETs works for the whole interval  $(0, 1)$ . What I am trying to say is that to notice that outer billiards on semi-regular octagons has a renormalization scheme, one has to enlarge the class of systems and consider the full range of octagonal PETs.

**Regular Polygons:** We have already discussed outer billiards on regular  $n$ -gons for  $n = 3, 4, 5, 8$ . The case  $n = 6$  resembles the cases  $n = 3, 4$  in that the periodic islands make a global and regular tiling. It is a good exercise to work out the picture. The cases  $n = 10$  and  $n = 12$  are similar to the cases  $n = 5, 8$ . One also has renormalization schemes in these cases. Bedaride and Cassaigne [BC] study the symbolic dynamics of these maps in detail.

Here is a recent general result whose deep proof has many new ideas about polygonal outer billiards.

**Theorem 3.3** *Outer billiards on the regular  $N$ -gon has aperiodic orbits as long as  $N \neq 3, 4, 6$ .*

This result is the main theorem in [KRTZ].

Beyond this result, and the ones mentioned above, not much is known about outer billiards on regular  $n$ -gons. Gordon Hughes has spent many years producing beautiful and intricate numerical studies of these. See [H].

### 3.3 The Pinwheel Map

In §2.6 we discussed a certain kind of sublattice PET which we called a strip map. Here we relate that construction to outer billiards. The results mentioned here are proved in [S8]. As in [S8] we work with polygons having no parallel sides. I have not carefully thought through the construction when  $P$  has some parallel sides, but I know how to do it for the regular octagon. See [S9].

**The Strips:** Each edge  $e$  of  $P$  defines an infinite strip  $X$ . One boundary component of  $X$  is the line extending  $e$ . The centerline of  $X$  contains the (unique) point of  $P$  farthest from  $e$ . Figure 3.6 shows the construction.

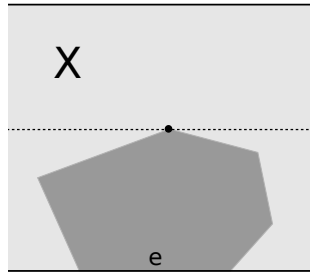


**Figure 3.6:** The strip  $X$  defined by  $(P, e)$ .

The  $n$ -gon  $P$  thus determines  $n$  strips, which we order cyclically, according to their slopes in  $\mathbf{R} \cup \infty$ . We label these strips  $X_0, X_2, \dots$ . See Figure 3.7 below.

**The Sublattices:** For each consecutive pair of strips  $(X_{k-1}, X_{k+1})$  there is a unique choice  $L_k = \mathbf{Z}v_k$  of sublattice such that

1.  $X_{k\pm 1}$  is a fundamental domain for  $L_k$ .
2. Lines parallel to  $v_k$  very far from the origin intersect  $X_{k-1}$  and  $X_{k+1}$  consecutively.

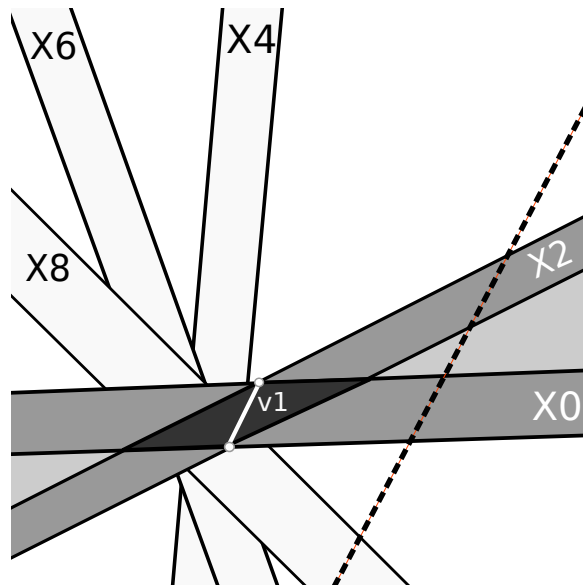


**Figure 3.7:** Defining the lattice  $L_1$  in terms of the strips.

Figure 3.7 shows the correct choice for an example. Here we are taking  $k = 1$ . We draw a segment for  $v_k$  instead of a vector because  $\pm v_k$  works here, independent of sign. We are not drawing the polygon  $P$  here; in fact we just made up this artificial example by putting down 5 strips

We introduce the “double wedge”  $W_k$  as the union  $\Sigma_{k-1}$  and  $\Sigma_{k+1}$  and the two infinite cones between these strips. This set is highlighted in Figure 3.7. (It is made from 4 different shades of grey.) Let  $f^2$  be the square of the outer billiards map  $f$ . The basic geometric principle is that if  $p \in W_k - X_{k+1}$ , and  $p$  is sufficiently far from the origin, then  $f^2(p) = p \pm v_k$ , where the sign is chosen so that  $p \pm v_k$  is one step closer to  $X_{k+1}$ .

**Shallow and Deep Equivalence:** The discussion above has the following consequence. If  $p \in X_0$  is very far from the origin then  $f^2$  moves  $p$  along a line parallel to  $v_1$  until the point lands in  $X_2$ , then  $f^2$  moves  $p$  along a line parallel to  $v_3$  until the point hits  $X_4$ , etc. When  $p$  is close to the origin, the relationship between the sublattice PET and  $f^2$  is more subtle, and we will discuss this below. Let  $\psi$  denote the second return map of  $f^2$  to  $X_0$ . The reason we consider the second return map is that we want to consider orbits which circulate all the way around  $P$  and not just halfway around. Let  $\psi^*$  denote the square of the PET defined by our decoration of the bipartite  $2n$ -cycle. We take the square here to match the behavior of  $\psi$ . We call  $\psi^*$  the *pinwheel map*.

**Theorem 3.4 (Shallow Equivalence)**  $\psi = \psi^*$  outside a compact subset of  $\mathbf{R}^2$ .

The proof of this result is essentially the discussion above. We call this *shallow equivalence*, because it is not very hard to prove.

We now mention the main result of [S8], which establishes a much deeper equivalence between the two maps.

**Theorem 3.5 (Deep Equivalence)** *There exists a large disk  $K \subset \mathbf{R}^2$ , centered at the origin, with the following two properties:*

- *Let  $p \in \mathbf{R}^2$  be any point for which the first  $n$  iterates of  $\psi$  are defined, and both  $p$  and  $\psi^n(p)$  are outside  $K$ . Then there is some  $n^* > 0$  such that the first  $n^*$  iterates of  $\psi^*$  are defined on  $p$  and  $(\psi^*)^{n^*}(p) = \psi(p)$ .*
- *Let  $p \in \mathbf{R}^2$  be any point for which the first  $n^*$  iterates of  $\psi^*$  are defined, and both  $p$  and  $(\psi^*)^{n^*}(p)$  are outside  $K$ . Then there is some  $n > 0$  such that the first  $n$  iterates of  $\psi$  are defined on  $p$  and  $\psi^n(p) = (\psi^*)^{n^*}(p)$ .*

The analogous result holds for  $n < 0$ . We have stated the case  $n > 0$  just for ease of exposition.

Theorem 3.5 says that near  $K$  the action of outer billiards and the pin-wheel map, though perhaps quite different from each other, is “removable”. The two different dynamical systems might do very different things to a point once it wanders into  $K$ , but the point emerges from  $K$  in the same way for both systems. I like to describe this theorem intuitively as saying that “what happens in Las Vegas stays in Las Vegas”. The unequal behavior of the two systems is entirely trapped in  $K$ , and it has no impact on what happens outside of  $K$ .

Theorem 3.5 immediately implies, for instance, that  $\psi$  has an unbounded orbit if and only if  $\psi^*$  has an unbounded orbit.

### 3.4 Quasi-Periodic Polygons

We call the polygon  $P$  *quasi-rational* if the associated sublattice PET is quasi-rational. Let us unpack this definition. The polygon  $P$  defines the strips  $X_0, X_2, \dots$  as above. We have the parallelograms  $\Pi_1, \Pi_3, \dots$  where

$$\Pi_k = X_{k-1} \cap X_{k+1}.$$

The polygon  $P$  is quasi-rational if it may be scaled so that all these parallelograms have integer areas. Semi-regular and regular polygons are all quasi-rational, and so are polygons whose vertices have rational coordinates.

Here is a well-known result about polygonal outer billiards.

**Theorem 3.6** *All the orbits are bounded for quasi-rational polygons.*

This result is the main result proved in 3 separate papers, namely [VS], [Ko], and [GS]. The essential idea in the proof is that there are certain periodic islands which fit together to make a “necklace” as in Figure 3.3. Each necklace surrounds the origin, and there are infinitely many necklaces of growing diameter. All the other orbits are trapped between consecutive necklaces, and this makes all the orbits bounded. Let me attempt my own proof; it essentially has the same idea as all the other proofs.

**Proof of Theorem 3.6:** We keep the notation from the previous section. We think of our sublattice PET as a product of parallelogram rotations, as described in §2.6. Because we are in the quasi-rational case, and as we

mentioned in §2.6, there is a single translation with respect to which all the parallelogram tilings are invariant. We call this the *grand translation*. The translation length is the least common multiplier of the widths of the parallelograms.

Let  $\mathcal{T}_k$  for  $k = 1, \dots, n$  be the  $n$  parallelogram tilings. Let  $\tau_k$  be the parallelogram in  $\mathcal{T}_k$  that contains the origin. Going back to the strip picture for moment, note that the intersection of all the the strips is precisely the polygon  $P$ . This means that  $\bigcap \tau_k = P$ . Call this the big intersection *the sweet spot*.

The map  $\psi^*$  acts as the identity on  $P$ . But then  $\psi^*$  acts as the identity on the image of  $P$  under any power of the grand translation. But then there are infinitely many translated copies of the sweet spot and this infinitely many translated copies of  $P$  on which  $\psi^*$  acts as the identity. Since  $\psi = \psi^*$  outside a compact set, there are infinitely many copies of  $P$  on which  $\psi$  acts as the identity. Figure 3.8 shows what this looks like.



**Figure 3.8:** Periodic array of copies of  $P$ .

Now we go back to the strip picture of the pinwheel map. By construction  $P$  has a unique vertex on the centerline of the strip  $X_0$ . Let  $Q$  be the result of reflecting  $P$  in this vertex. Let  $P'$  be any copy of  $P$  in our periodic array that is sufficiently far from the origin. By construction,  $f(P') = Q'$ , where  $Q'$  is the corresponding copy of  $Q$ . Here  $f$  is the outer billiards map. Figure 3.9 shows  $f^{2k}(P')$  for  $k = 0, 1, 2, 3$  and  $f^{2k}(Q')$  for  $k = 0, 1, 2$ . By construction, the consecutive images share a vertex in common.

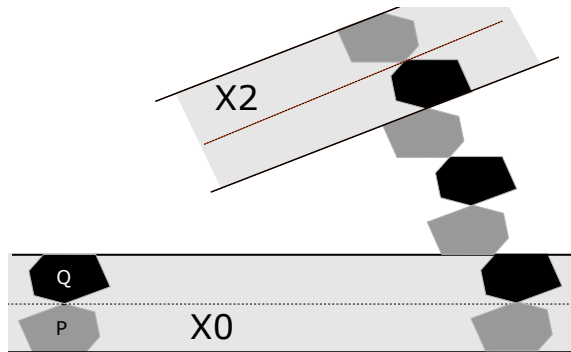


**Figure 3.9:** The formation of a necklace

We have depicted the case when  $f^4(Q') \in X_2$ . In general there will be some first  $k > 0$  when either

- $f^{2k}(P') \in X_2$  and all previous polygons lie in  $W_1 - X_2$ .
- $f^{2k}(Q') \in X_2$  and all previously defined polygons lie in  $W_1 - X_2$ .

The choice of  $P'$  or  $Q'$  depends on whether or not the edges defining  $X_0$  and  $X_2$  are adjacent or not. We are showing the non-adjacent case. In either case, we now consider the images between  $X_2$  and  $X_4$ . The significant thing is that  $P$  sits inside  $X_2$  just as it sits inside  $X_0$ . Repeating all the same steps, we see that the orbit of  $P'$  continues into  $W_3$ , starting and stopping in  $X_2$  and  $X_4$ .

Continuing all the way around, we produce a necklace orbit, one consisting of cyclically tangent isometric copies of  $P$ . Compare Figure 3.2. But we can make this construction for any  $P'$  sufficiently far from the origin. This gives us an infinite sequence of necklace orbits. All other orbits are trapped between the necklaces and hence bounded. Compare Figure 3.3. ♠

**The Rational Case:** Theorem 3.6 has a very appealing corollary.

**Theorem 3.7** *When the vertices of  $P$  are rational, all the outer billiards orbits of  $P$  are periodic.*

**Proof:** When  $P$  has rational vertices, we can scale so that all the vertices have integer coordinates. The map  $f^2$  is then a piecewise translation involving a finite number of integer vectors. In particular, if we start with any point  $p \in \mathbf{R}^2 - P$  with a well-defined orbit, the orbit of  $p$  is bounded and consists of points which differ from  $p$  by integer vectors. Hence, this orbit must be finite. Hence, all orbits are periodic in this case. ♠

This is an especially appealing situation, because every rational polygon gives rise to a dynamically invariant tiling of  $\mathbf{R}^2$  by periodic islands.

**Existence of Periodic Orbits:** C. Culter proved <sup>2</sup> the following result.

**Theorem 3.8 (Culter)** *Outer billiards has a periodic orbit outside every compact subset of  $\mathbf{R}^2$  with respect to any polygon.*

---

<sup>2</sup>I don't know if Culter ever wrote a paper about his result, but see [T1] for an account

**Proof:** (sketch) When the sublattice PET is quasi-rational, the necklace orbits furnish infinitely many periodic points. In the general case, we see an infinite sequence of polygons in  $X_0$  which converge to  $P$  up to translations of  $X_0$ . Each such polygon is the intersection of the parallelograms in the tiling that contain it. For this reason  $\psi^*$  is the identity on such polygons. But then, by the shallow equivalence, the same is true for  $\psi$  far from the origin. This gives periodic orbits outside any compact set. ♠

### 3.5 The Arithmetic Graph

In this section we work with the pinwheel map. Suppose we have a  $n$ -gon  $P$  on which the outer billiards map and the pinwheel map are defined. Let  $p_0 \in X_0$  be some point with a well-defined orbit. Referring to Equation 6, define

$$p_{2k+2} = \phi_{b_{2k+1}w_{2k+1}b_{2k}}(p_{2k}) \in X_{2k+2}.$$

We mean to define this for  $k = 1, \dots, 2n$  and we take the indices cyclically mod  $2n$ . These points are just successive images of  $p_0$  under the pinwheel map.

There is a non-negative integer  $N_k$  such that  $p_{2k+2} - p_{2k}$  is  $N_k$  times one of the two generators of the sublattice  $L_{2k+1}$ . We define the *spectrum* of  $p$  to be the length- $n$  vector

$$S(p) = (N_0 - N_{2n}, N_2 - N_{2n+2}, \dots, N_{2n-2} - N_{4n-2}) \in \mathbf{Z}^n. \quad (10)$$

Experimentally, all the entries in  $S(p)$  lie in  $\{-1, 0, 1\}$ , but I don't know if this always happens. The length of the spectrum is  $n$ .

Supposing that we have chosen a linear projection  $\Lambda : \mathbf{R}^n \rightarrow \mathbf{C}$  we define the  $\Lambda$ -spectrum of  $p$  to be  $\Lambda \circ S(p)$ . One choice of projection is given by

$$\Lambda_k(S) = \sum_{k=1}^n S_k \omega^k, \quad \omega = \exp(2\pi ki/n). \quad (11)$$

We call the corresponding spectrum  $\Lambda_k \circ S$  the *k-cyclotomic spectrum*.

Assuming we have fixed  $\Lambda$ , we can associate to a periodic point  $p$  a periodic path  $\Lambda(p) \subset \mathbf{C}$ . Letting  $\{p^k\}$  be the  $\psi^*$ -orbit of  $p = p^0$ , we form the path whose vertices are

$$\Lambda \circ S(p^0), \quad \Lambda \circ S(p^0) + \Lambda \circ S(p^1), \quad \Lambda \circ S(p^0) + \Lambda \circ S(p^1) + \Lambda \circ S(p^2), \dots$$

When we use the  $k$ -cyclotomic spectrum, we call  $\Lambda(p)$  the  $k$ -cyclotomic graph of  $p$ . The cyclotomic case is adapted to the case of regular polygons.

We now return to outer billiards on the regular pentagon. Recall that this system has two kinds of periodic islands: pentagonal and decagonal. Figure 3.11 shows the 2-cyclotomic graph for a pentagonal periodic island on the left and for a decagonal periodic island on the right. One should compare this with Figure 2.7.

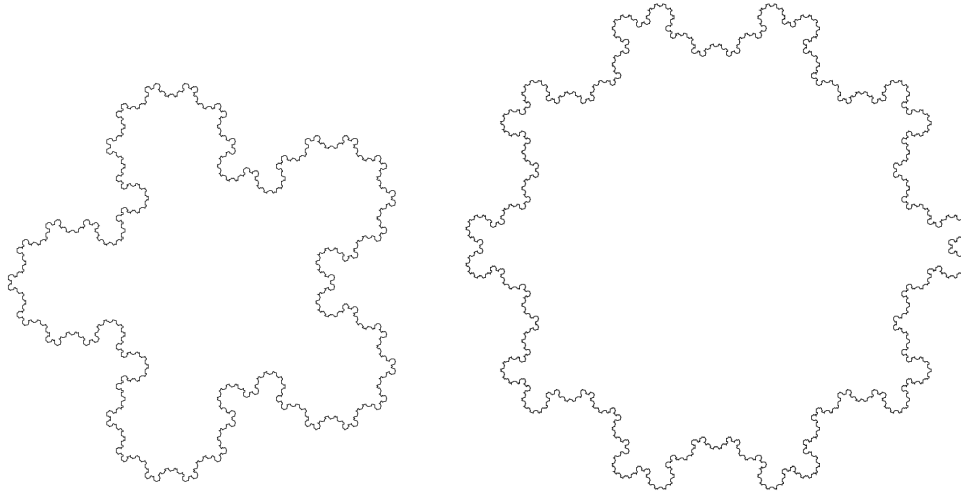


**Figure 3.10:** The 2-cyclotomic graph in the regular pentagon case

The 3-cyclotomic graph looks the same. The 1-cyclotomic graph and the 4-cyclotomic graph are not interesting; they essentially just reproduce the orbit. I did not attempt to prove that these curves have the beautiful structure shown in Figure 3.10, but I could imagine a proof whose first step is to condense the generation of these curves into the kind of short Mathematica program (i.e. substitution rule) that I presented in §2.3. An analysis of the renormalization scheme would give the substitution rule, and then a direct geometric analysis would establish the general features of the picture. I leave this to the interested reader.

My computer program makes sense of the pinwheel map for regular octagons, and in this case [S9] I worked out all the details (justifying the appearance of the pictures) in extreme detail. For the regular octagon the 2-cyclotomic graph and the 3-cyclotomic graph are different. Figure 3.11 shows what the 3-cyclotomic graph looks like. This is quite similar to what happens for the regular pentagon.

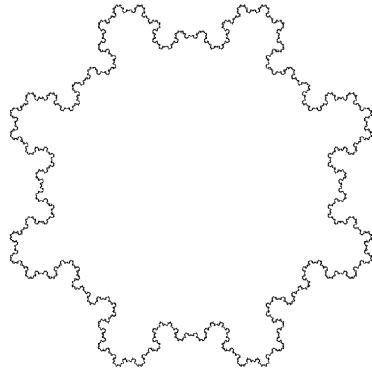


**Figure 3.11:** The 3-cyclotomic graph in the regular octagon case

Figure 3.12 shows the two typical pictures of the 2-cyclotomic graph for long periodic orbits. The first case is a closed polygon, though not embedded. The rescaled limit of this thing is an object somewhat reminiscent of the classic square Sierpinski carpet. The second case is an open polygonal path, and we are showing several periods of it.

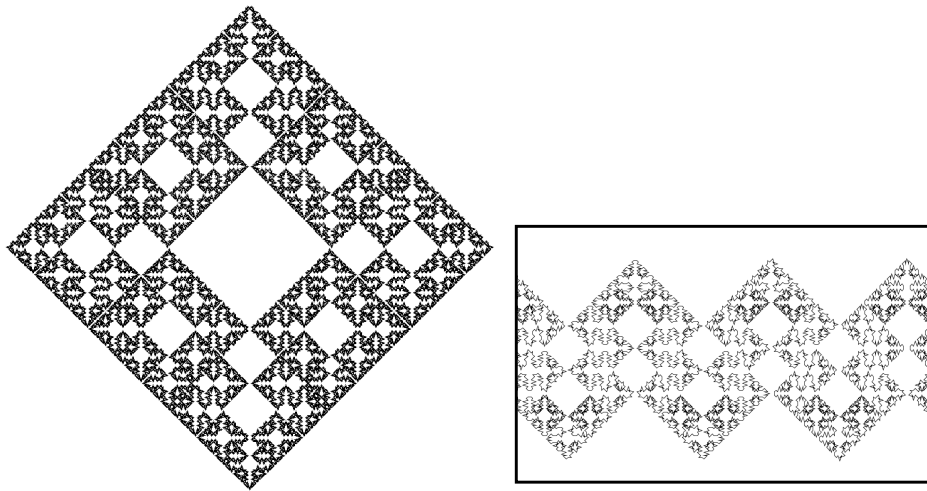


**Figure 3.12:** The 2-cyclotomic graph in the regular octagon case

I wrote a long article [S9] exploring the arithmetic graph in the regular octagon case, though I never published it. My program also draws the cyclotomic graphs with respect to other regular polygons. The interested reader can play around with the software (or write their own) and see other neat pictures.

## 4 Unbounded Orbits for Outer Billiards

### 4.1 Some Results and Questions

The Moser-Neumann problem [N], [M1], [M2] asks about the existence of unbounded orbits for outer billiards. I have already mentioned the result [VS], [Ko], [GS] that all orbits are bounded for quasi-rational polygons. Another result along these lines, due to Dan Genin [Ge], is that all orbits are bounded for trapezoids. Trapezoids fall outside the quasi-rational framework. See the introduction of [S3] for a survey of other boundedness results for non-polygonal shapes.

I answered the Moser-Neumann question in 2007 by proving that outer billiards on the Penrose kite has an unbounded orbit. See [S5]. The Penrose kite is the convex quadrilateral that arises in the famous Penrose kites-and-darts tiling. I showed, in particular, that the point  $p$  in Figure 4.1 has a well defined and unbounded orbit when outer billiards is defined with respect to the kite shown in Figure 4.1. The auxiliary lines in the picture are present to show the construction of the kite and the special point.

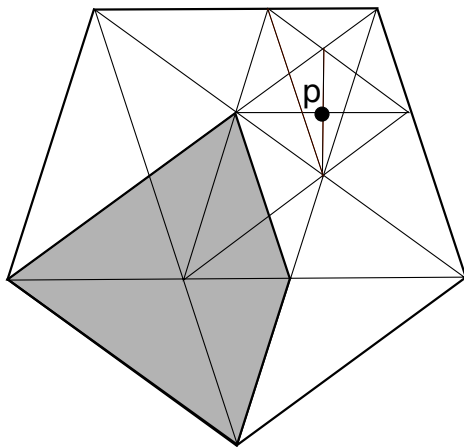


**Figure 4.1:** The Penrose kite and a point with an unbounded orbit.

My initial proof of this result exploited a quasi-self-similarity property of the arithmetic graph associated to this orbit. See Figure 4.5 below. Initially I derived this by hand, in some sense. Later on, I found a renormalization scheme which explained this. I will discuss all this below.

In [S3] I proved a more general result concerning the kites  $K(A)$  having vertices  $(-1, 0)$  and  $(0, \pm 1)$  and  $(A, 0)$  with  $A \in (0, 1)$ . The Penrose kite is

affinely equivalent to  $K(\sqrt{5}-2)$ . Note that  $K(A)$  is a rational polygon when  $A \in \mathbf{Q}$  and not quasi-rational when  $A \in \mathbf{R} - \mathbf{Q}$ . Here is the main result from [S3].

**Theorem 4.1** *Outer billiards on  $K(A)$  if and only if  $A \in (0, 1) - \mathbf{Q}$ .*

The orbits I found all lie on the set  $\Sigma = \mathbf{R} \times \mathbf{Z}_{\text{odd}}$ , where  $\mathbf{Z}_{\text{odd}}$  is the set of odd integers. In [S3] I provide quite a bit of fine-grained information about the unbounded orbits. For instance

**Theorem 4.2** *The following is true.*

- *Any unbounded orbit in  $\Sigma$  enters every neighborhood of the points  $(0, \pm 1)$ . In particular, this orbit intersects the set  $(0, 2) \times \{1\}$ .*
- *The set  $C$  of points in  $(0, 1) \times \{1\}$  with unbounded orbits equals a Cantor set up to deleting a countable number of points.*
- *The first return map to  $C$  is conjugate in an explicit way to the “plus one map” in a procyclic group. The procyclic group depends on  $A$ .*

A *procyclic group* is the inverse limit of finite cyclic groups. What this means is that we have an infinite chain  $\dots C_2 \rightarrow C_1 \rightarrow C_0$ , of finite cyclic groups of unboundedly growing order, such that each arrow is a surjective group homomorphism. The procyclic limit is the group of all sequences  $\{a_n\}$  with  $a_n \in C_n$  and  $a_n \rightarrow a_{n-1}$  for all  $n$ . The “plus one map” is the map  $x \rightarrow x + 1$  acting on this space.

I will illustrate some of this structure in the next section. I discovered essentially every result about outer billiards on kites by making and then using a massive graphical user interface *Billiard King*. You can get Billiard King here.

<https://www.math.brown.edu/reschwar/BilliardKing/index.html>

The best way to learn about my work in [S3] is to download *Billiard King* and play around with it. In this modern era of A.I., you can get a program like chatGPT or Claude or Gemini to guide you to installing and running this program.

Shortly after [S3], D. Dolgopyat and B Fayyad [DF] proved that outer billiards has unbounded orbits when defined relative to a semi-disk, the set you get when you cut a disk in half. They also proved this result for the sets you get when you nearly cut the disk in half. Their methods are completely different, and their unbounded orbits march straight out to infinity.

These are the only known unboundedness results. One natural question is:

**Conjecture 4.3** *Outer billiards has unbounded orbits with respect to almost every polygon.*

Here is a more precise conjecture:

**Conjecture 4.4** *Suppose that  $P$  is a convex polygon with no parallel sides. If  $P$  is not quasi-rational then outer billiards has unbounded orbits with respect to  $P$ .*

This second conjecture is so strong that I am not completely certain it is true. One should probably just take it as a question.

## 4.2 The Kite Result Illustrated

In this section I am going to use the arithmetic graph to give some ideas behind my result about unbounded orbits for outer billiards on irrational kites. In discussing the ideas, I will depart somewhat from the treatment in [S3] in order to better relate to the ideas we have presented above. My idea is to present things here in a way that might generalize more naturally than the special treatment given in [S3].

The first idea in our analysis is to understand what happens for  $K(A)$  when  $A = p/q$  is rational. The idea is to approach an irrational  $A$  with a controlled sequence of rationals and to take a suitable limit of the dynamics in the rational case. In our proof we work with  $pq$  odd but here we will show pictures for  $pq$  even. The pictures are nicer. We let  $\psi_A$  denote the pinwheel map associated to  $K(A)$ , and (referring to the arithmetic graph construction in the previous chapter) we let  $\Lambda(S_0, S_1, S_2, S_3) = (-S_0, S_2)$ . Note that the spectrum has the same length as the number of sides as the polygon – four in this case. We define the arithmetic graph relative to this choice of  $\Lambda$ . The set  $\Sigma$  is invariant under the outer billiards map, and so it makes sense to look for unbounded orbits on this set. We label so that  $X_0$  is the strip shown in Figure 4.2.

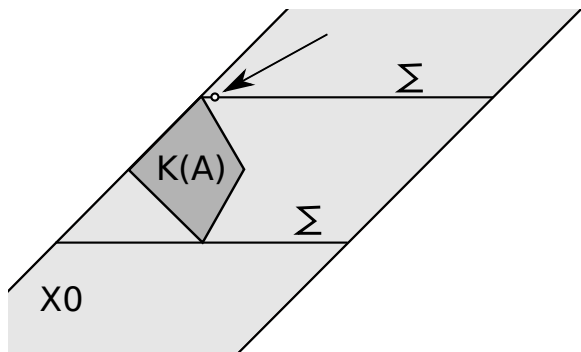


**Figure 4.2:**  $\Sigma \cap X_0$ , and the fundamental start.

Given the deep equivalence between outer billiards and pinwheel map – a result which is quite easy to prove for kites – it suffices to prove that  $\psi : X_0 \cap \Sigma \rightarrow X_0 \cap \Sigma$  has unbounded orbits. This map is an infinite interval exchange transformation. When  $A = p/q$ , all the intervals in the exchange have length which is an integer multiple of  $2/q$ . For this reason, all points in the set

$$(0, 2/q) \times \{1\} \tag{12}$$

have the same combinatorial orbit. We call the point  $(1/q, 1)$  the *fundamental start* and its pinwheel orbit the *fundamental orbit*. We will show pictures of the arithmetic graph of the fundamental orbit.

We first mention a few general features of these paths. The arithmetic graphs are all *lattice polygonal paths*. That is, their vertices are integer points. I proved in [S3] that the arithmetic graphs are embedded, and that consecutive vertices are always adjacent in  $\mathbf{Z}^2$ . That is, each coordinate of a given point differs by at most 1 from the corresponding coordinate of the adjacent points. Given the integer nature of the path, a fractal-looking example much be really huge. The point is that such a monster is meant to be scaled so that its vertices are integral.

Define the *baseline* to be the line of slope  $-A$  through the origin.

**Lemma 4.5** *The distance between a point on the arithmetic graph and the baseline is comparable to the distance from the corresponding point in the orbit to the origin.*

**Proof:** This is a result more easily seen in the coordinates given in [S3, §2.6]. The basic idea is that the map from the arithmetic graph to the dynamical

plane very nearly sends the point  $(m, n)$  to the point  $(2Am + 2n + 1/q, \pm 1)$ . Here we are taking  $A = p/q$  as above. The line of slope  $-A$  through the origin maps to  $(1/q, \pm 1)$  and then points increasingly far from this line map increasingly far away from the origin. ♠

Thus, if the arithmetic graph is very tall, then some points in the orbit are very far from the origin. We are interested in finding points having an arithmetic graph that rises unboundedly far above the baseline.

Likewise we have the following result.

**Lemma 4.6** *The points of the arithmetic graph that are within 1 unit of the baseline correspond to the intersection of the orbit with the special interval  $(0, 2) \times \{1\}$ .*

**Proof:** This has essentially the same proof as the previous lemma, and is most easily seen from the explicit map given in [S3, §2.6]. ♠

Now we show some pictures. Again, when  $A = \sqrt{5} - 2$  the kite  $K(A)$  is affinely equivalent to the Penrose kite. The first 4 continued fraction approximations to  $A$  are  $1/4$  and  $4/17$  and  $17/72$  and  $72/305$ . The numbers  $1, 4, 17, 72, 305$  satisfy the recurrence relation  $a_{n+2} = 4a_n + 1$ , and the pattern continues. Figure 4.3 below shows the arithmetic graph of the fundamental orbit for these first 4 fractions.

It looks like these pictures are converging to a fractal. However, this is just because we are rescaling the picture so that it always fits on the page. In the natural scale, where the edges have about unit length, the heights of these pictures tend to  $\infty$ . This strongly suggests that there are unbounded orbits. However, we cannot take the limit of the fundamental starting point, because this point converges to the kite vertex as the approximating rational converges to  $\sqrt{5} - 2$ .

We need to take a limit in a careful way. As we explain in [S3], we need to have a sequence  $\{p_n/q_n\}$  rationals where a significant portion of the graph  $\Gamma_{n+1}$  coincides (or, so to speak “copies”) a significant portion of the graph  $\Gamma_n$ . We call this phenomenon *period copying*. If you look carefully at Figure 4.3, you can see that a significant portion of the bottom part of each graph is copied by the next graph in the progression. Figure 4.4 shows this copying phenomenon more clearly.

To get an idea of why this periodic copying might be necessary, think about the familiar phenomenon from real analysis, in which the 0-function can be the pointwise limit of a sequence of functions whose sup-norm tends to  $\infty$ . To get an unbounded limit, we need more control on the nature of the convergence.

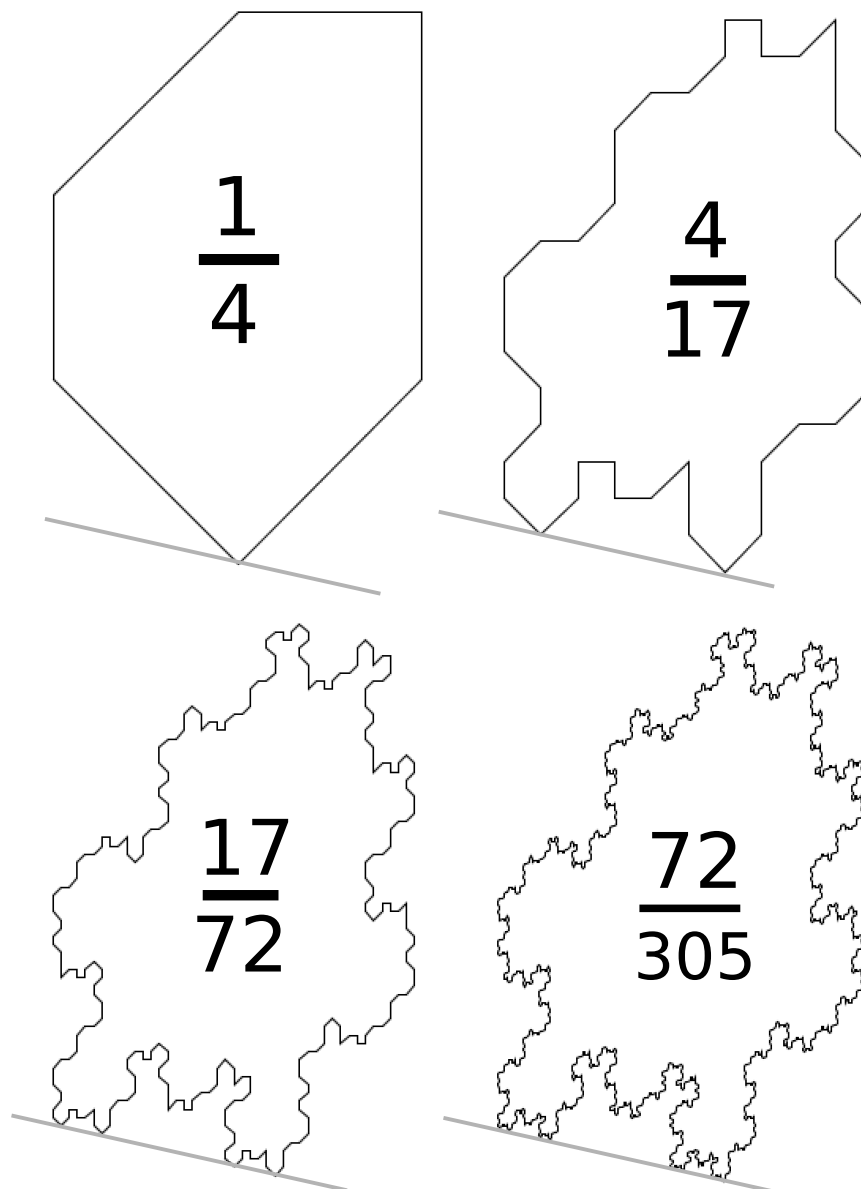


**Figure 4.3:** The arithmetic graph for  $1/4$ ,  $4/17$ ,  $17/72$ , and  $72/305$ .

There is something else to notice about these pictures. The bottom parts of the picture seem to be touching – or, rather, nearly touching – the baseline in a Cantor set. This kind of structure (in the general case) is responsible for the second statement in Theorem 4.2. A careful analysis of how these figures rise up and return down to the baseline (in the general case) is responsible for the third statement in Theorem 4.2.

Here is another especially pretty one. The rational  $408/985$  is a continued fraction approximant of  $\sqrt{2} - 1$ . One can see the same kind of Cantor set formation near the baseline.

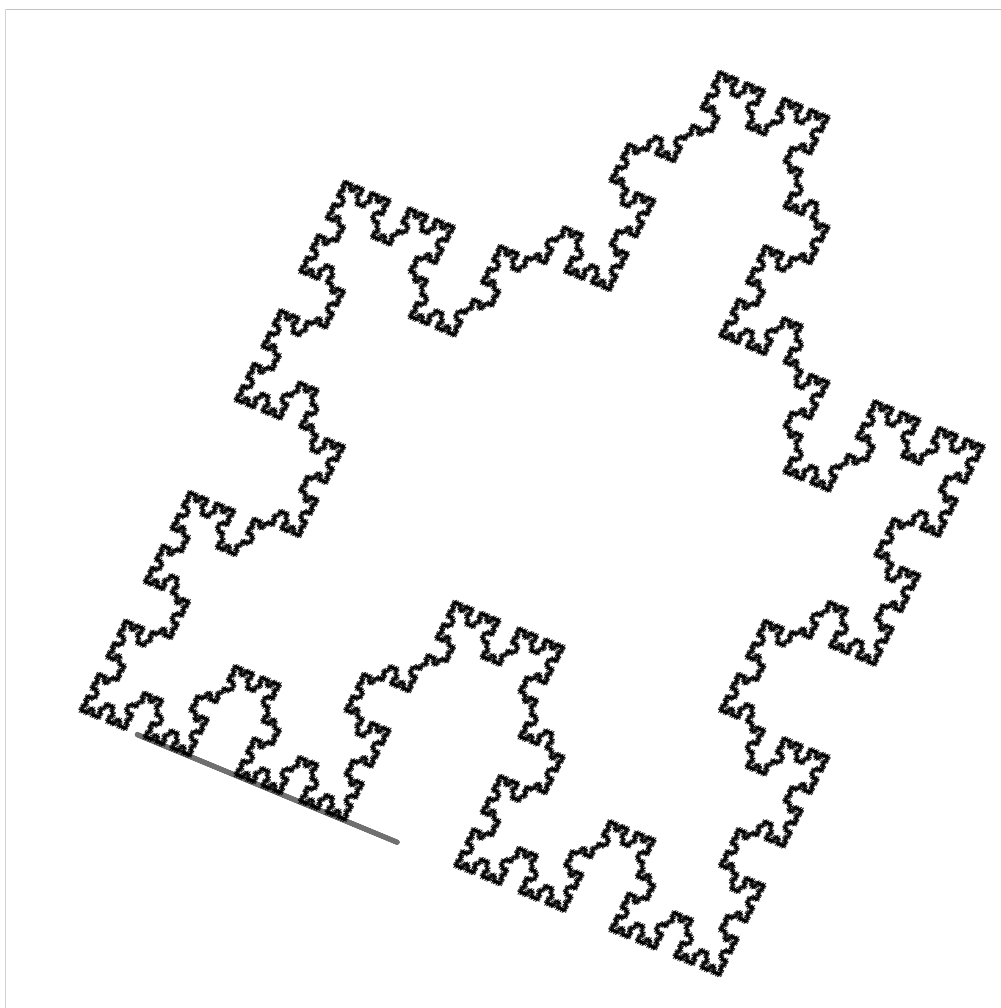
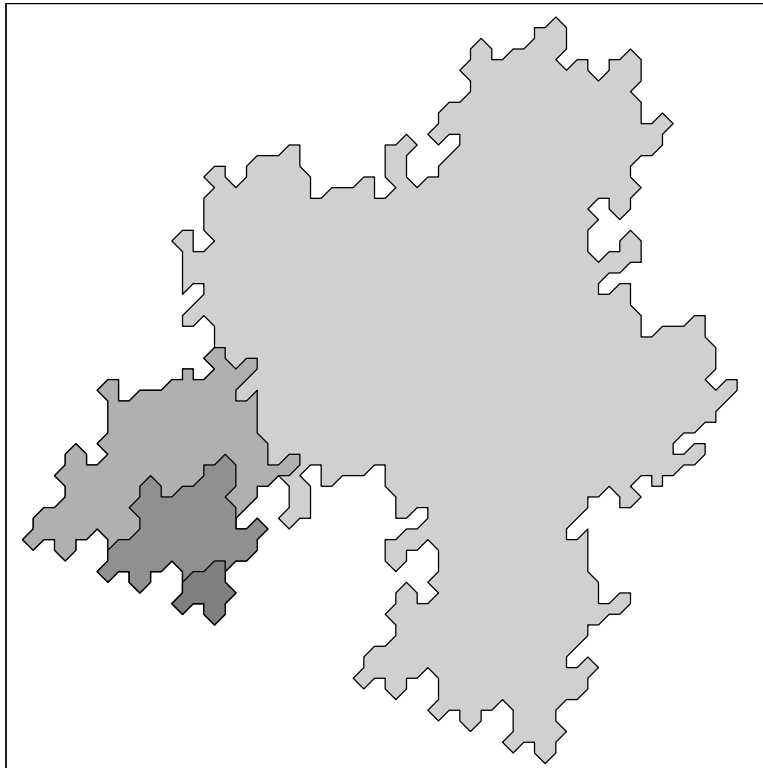


Figure 4.4: The arithmetic graph for  $408/985$ .

The numbers  $\sqrt{5} - 2$  and  $\sqrt{2} - 1$  are fixed points of a certain renormalization operator that is similar to the one  $R$  described in §2.5. For a general choice of irrational  $A$  we also observe this Cantor set phenomenon, but the Cantor set is not as regular. The reader can see their own pictures using my program *Billiard King*.

Let me illustrate the general phenomenon with one example. Two rationals  $p_1/q_1$  and  $p_2/q_2$  are *Farey adjacent* if  $|p_1q_2 - p_2q_1| = 1$ . The 4 rationals involved in the next picture are consecutively farey adjacent. We plot the corresponding 4 arithmetic graphs at the same scale. One can see that the consecutive polygons are nested inside of each other. Each one is somehow part of the next one.



**Figure 4.4:** The arithmetic graph for  $2/5$  and  $5/12$  and  $8/19$  and  $21/50$ .

This general nesting phenomenon is related both to the Cantor set phenomenon discussed in Theorem 4.2 and also to the period copying phenomenon discussed in connection with the idea of analyzing outer billiards on an irrational kite by taking the limit of what happens in a sequence of rational approximants.

I want to emphasize that this is really just an impressionistic account of [S3], which fills a research monograph. In particular, one thing I should say is that I did not actually establish the strict nesting property you see in Figure 4.4. Even though I did not prove it, it seems that this strict nesting phenomenon always happens. Rather, I considered the graphs corresponding to rationals of the form  $p/q$  with  $pq$  odd, and I proved that the larger graph copies the bottom part of the smaller graph. What I am trying to say is that you see some extra-beautiful phenomena in the pictures which I did not actually prove. I just proved enough to prove results like Theorem 4.2 and other results contained [S3].

### 4.3 Compactification

Now, let  $\psi^* : X_0 \rightarrow X_0$  be the pinwheel map considered in the previous chapter. We insist that the underlying polygon is not quasi-rational. In [S6] I prove the following result.

**Theorem 4.7** *There exists a double lattice PET  $\widehat{\psi} : \widehat{X}_0 \rightarrow \widehat{X}_0$  and an injective semi-conjugacy  $\Theta : X_0 \rightarrow \widehat{X}_0$ . That is,  $\widehat{\psi} \circ \Theta = \Theta \circ \psi^*$ . The dimension of the image closure is the  $\mathbf{Q}$ -rank of the list  $A_1, \dots, A_n$  of areas of parallelograms associated to  $\psi^*$ .*

We defined double lattice PETs at the end of §2.4.

Generically, the  $\mathbf{Q}$ -rank is  $n$ , the number of parallelograms, and the map  $\Theta$  has dense image. The punchline here is that generically the pinwheel map, which is essentially the same as outer billiards, is induced by considering the action of a PET, whose domain is a compact set, on a (typically) dense 2-dimensional subspace, and then identifying this subspace with the domain for the pinwheel map. In other words, we are putting a non-compact system inside a higher dimensional compact system. This is why I call this a *compactification*.

All this specializes to the case of kites. In [S3] and [S4] I studied the kite case of the compactification in great detail, but only for the restriction of  $\psi^*$  to  $X \cap \Sigma_0$ . That is, I studied the compactification of an infinite IET. (I wrote [S3] first, and this gave me the idea for the generalization in [S6]. )

In the case studied in [S3] and [S4], namely the compactification of a 1-dimensional infinite IET, the compactification is 2-dimensional when the parameter is a quadratic irrational, and 3-dimensional when the parameter is neither rational nor quadratic irrational. So, for the generic choice of

$A \in (0, 1)$  the infinite IET has a 3-dimensional compactification which I call  $\widehat{X}_A$ .

My *Master Picture Theorem* in [S3] shows that  $\widehat{X}_A$  is (generically) a 3-dimensional slice of a 4-dimensional convex polytope  $\widehat{X}$  with integer coordinates. The partitions which go into the map on  $\widehat{X}_A$  fit together to give two partitions of  $\widehat{X}$  into smaller convex polytopes with integer coordinates. The PET maps fit together as well, and give rise to a piecewise affine map which carries each piece of one partition on  $\widehat{X}$  to the corresponding piece of the other partition. My computer program *Billiard King* allows you to visualise these 4D partitions by plotting slices of them.

Referring back to §2, this 4-dimensional *Master PET* is a piecewise- $\mathcal{A}$  map where  $\mathcal{A}$  is the set of affine transformations. These affine transformations have the special property that certain of their 3-dimensional slices, the ones just mentioned, are translations.

The large scale structure of the arithmetic graph is a consequence of the properties of this 4-dimensional polytope and its partitions. For instance, the reason that the bottom parts of the arithmetic graphs agree for Farey related rationals is that we compute the two dynamical picture by looking at two nearby slices of the master 4D system. These slices are very close in comparison to the size of the interval, namely  $2/q$ , involved in the fundamental orbit.

The compact PET associated to the Penrose kite parameter  $A = \phi^{-3}$  is 2 dimensional, and it has a renormalization scheme. This is how I first proved that outer billiards has an unbounded orbit relative to the Penrose kite. Figure 4.5 shows the arithmetic graph for the orbit of the point  $p$  shown in Figure 4.1. The graph itself is shown in black and then the grey path is a rescaled version. The rescaling factor is  $\phi^3$ . The renormalization scheme I found implies that the corresponding arithmetic graphs are quasi-self similar. That is, the arithmetic graph for one of these unbounded orbits lies in a bounded tubular neighborhood of a dilated copy of the same arithmetic graph. This dilation structure also implies that the unbounded orbit itself is locally self-similar.

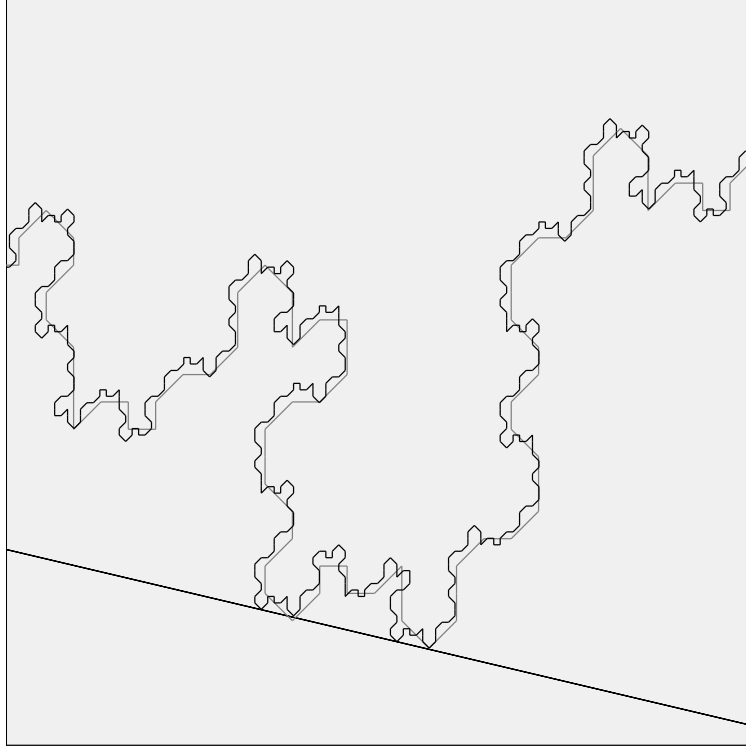


**Figure 4.5:** Quasi-self-similarity for the arithmetic graph.

In [S10] I found a more elaborate renormalization scheme that works for all the orbits relative to the Penrose kite, and not just the special ones discussed above. Here are some of the results I got concerning all the orbits relative to the Penrose kite. Before stating the result, I want to emphasize that the results from [S3] only concern the unbounded orbits on lines of the form  $\mathbf{R}_y = \mathbf{R} \times \{y\}$  where  $y$  is an odd integer.

**Theorem 4.8** *The following is true about outer billiards orbits relative to the Penrose kite.*

1. *Every defined orbit is either unbounded in both directions or periodic.*
2. *The set of points with unbounded orbit has Hausdorff dimension 1.*
3. *The set of  $y$  such that  $\mathbf{R}_y$  has an unbounded orbit is a Cantor set of Hausdorff dimension  $\log 3 / \log(\phi^3)$ .*
4. *Suppose that  $y = m + n\phi$  where  $\phi$  is the golden ratio and  $m, n \in \mathbf{Z}$ . Then  $\mathbf{R}_y$  has unbounded orbits if and only if  $m$  is odd and  $n$  is even.*

## 4.4 Compactification and Renormalization

One of my dreams is that the Master PET discussed in the previous section, or the larger 5-dimensional version which comes from looking at the whole pinwheel map and not just the restriction to  $\Sigma$ , has a renormalization scheme like the octagonal PETs. This would be a different way to explain some of the self-similar properties of the arithmetic graph. This kind of renormalization scheme would bring the study of outer billiards on kites more in line with the study of the octagonal PETs.

Going further, I think it would be great to have a renormalization scheme for double lattice PETs in general. There is some hope, because these objects are closely associated with the general linear groups. I imagine something along the lines of multi-dimensional continued fractions, a higher dimensional version of Rauzy induction.

In summary, here is my idea about a 4-step plan to understand the question of unbounded orbits in polygonal outer billiards.

1. Replace outer billiards with the pinwheel map. See [S8].
2. Compactify the pinwheel map. The result, at least generically, is a double lattice PET. See [S6].
3. Look for general renormalization scheme for double lattice PETs, along the lines of Rauzy induction for interval exchange transformations. See [S0] for the Penrose kite.
4. Encode the dynamics of the double lattice PET using the arithmetic graph. See [S6] and also a deep exploration of this in [S4] for kites.

I had always hoped to carry out some steps of this program, but so far I have not done this.

## 5 References

- [**BC**], N. Bedaride, J. Cassaigne, *Outer billiard outside regular polygons*, Journal of the London Math Society (2011)
- [**DF**] D. Dolyopyat and B. Fayad, *Unbounded orbits for semicircular outer billiards*, Annales Henri Poincaré, to appear.
- [**FM**], G. Forni and C. Mateus, *Introduction to Teichmüller Theory and its applications to dynamics of interval exchange transformations, flows of surfaces, and billiards*, arXiv:1311.2758
- [**Ge**] D. Genin, *Regular and Chaotic Dynamics of Outer Billiards*, Pennsylvania State University Ph.D. thesis, State College (2005).
- [**Go**], A. Goetz, *Piecewise Isometries: An Emerging Area of Dynamical Systems* (2003)
- [**GS**] E. Gutkin and N. Simanyi, *Dual polygonal billiard and necklace dynamics*, Comm. Math. Phys. **143**:431–450 (1991).
- [**H**] G. Hughes, *Outer Billiards on Regular Polygons*, (2013) arXiv:1311.6763
- [**Ke**] M. Keane, *Interval exchange transformations*, Math Z. **141** (1975) pp. 25–31
- [**Ko**] Kolodziej, *The antibilliard outside a polygon*, Bull. Pol. Acad Sci. Math. **37**:163–168 (1994).
- [**KRTZ**], A. Kanel-Belov, P Rukhovich, V. Timorin, V. Zgurskii, *Aperioric points for dual billiards* (2023) arXiv: 2311.09643
- [**M1**] J. Moser, *Is the solar system stable?*, Math. Intelligencer **1**:65–71 (1978).
- [**M2**] J. Moser, *Stable and random motions in dynamical systems, with special emphasis on celestial mechanics*, Ann. of Math. Stud. 77, Princeton University Press, Princeton, NJ (1973).

- [N] B. H. Neumann, *Sharing ham and eggs*, Summary of a Manchester Mathematics Colloquium, 25 Jan 1959, published in Iota, the Manchester University Mathematics Students' Journal.
- [R], G. Rauzy, *Échanges d'intervalles et transformations induites*, Acta Arithmetica **34(4)** (1979) pp 315-328
- [S1] R. E. Schwartz, *Survey Lecture on Billiards*, Proceedings of the International Congress of Mathematicians (2022)
- [S2] R. E. Schwartz, *Continued Fractions and the Four Color Theorem*, Journal of Experimental Mathematics, Issue 1 (2023) to appear.
- [S2] R. E. Schwartz, *Outer Billiards on Kites*, Annals of Mathematics Studies **171** (2009)
- [S4] R. E. Schwartz, *The Plaid Model*, Annals of Mathematics Studies **198** (2018)
- [S5] R. E. Schwartz, *Unbounded Orbits for Outer Billiards*, J. Mod. Dyn. **3**:371–424 (2007).
- [S6] R. E. Schwartz, *Outer Billiards, Polytope Exchange Transformations, and Quarter Turn Compositions*, Preprint (2011)
- [S7] R. E. Schwartz, *The Octagonal PETs*, A. M. S. Research Monograph (2013).
- [S8] R. E. Schwartz, *Outer Billiards and the Pinwheel Map*, J. Modern Dynamics **2** (2011) pp 255-283
- [S9] R. E. Schwartz, *Outer Billiards, the Arithmetic Graph, and the Octagon*, preprint (2010)
- [S10] R. E. Schwartz, *Outer Billiards and the Penrose Kite: Compactification and Renormalization*, J. Modern Dynamics **3** (2012) pp 473-581

- [**T0**] S. Tabachnikov, *Geometry and billiards*, Student Mathematical Library 30, Amer. Math. Soc. (2005).
- [**T1**] S. Tabachnikov, *A proof of Culter’s theorem on the existence of periodic orbits in polygonal outer billiards*, *Geometriae Dedicata* **129**(1):83–87 (2007).
- [**T2**] S. Tabachnikov, *Billiards*, Société Mathématique de France, “Panoramas et Synthèses” 1, 1995
- [**VL**] F. Vivaldi and J. H. Lowenstein, —it Arithmetical properties of a family of irrational piecewise rotations, *Nonlinearity* **19**:1069–1097 (2007).
- [**VS**] F. Vivaldi and A. Shaidenko, *Global stability of a class of discontinuous dual billiards*, *Comm. Math. Phys.* **110**:625–640 (1987).
- [**Z**] A. Zorich, *Flat Surfaces*, *Frontiers in Number Theory, Physics, and Geometry*, Vol 1, ed. P. Cartier; B. Julia; P. Moussa; P. Vanhove, Spr.-Verlag (2006)